Spin-Exchange Cross Sections for Rb^{87}-Rb^{87} and Rb^{87}-Cs^{133} Collisions*

HYATT M. GIBBS AND ROBERT J. HULL†
Lawrence Radiation Laboratory and Department of Physics, University of California, Berkeley, California

(Received 29 June 1966)

In a hyperfine-optical-pumping experiment we employed the Franzen transient method to determine the total spin-exchange cross sections for Rb^{87}-Rb^{87} and Rb^{87}-Cs^{133} collisions at 78°C. Values determined in this way were: $\sigma(Rb^{87}\text{-}Rb^{87})=(1.9\pm0.2)\times10^{-14}$ cm² and $\sigma(Rb^{87}\text{-}Cs^{133})=(2.3\pm0.2)\times10^{-14}$ cm². A large difference between the ground-state hyperfine populations was established by pumping with light absorbable by atoms in only one hyperfine level. In the presence of a second unpumped species, the resulting polarization relaxed with a characteristic rate of $1/\tau=1/T+1/T_{S1}+1/T_{E1}$, where T is the non-spin-exchange relaxation time and T_{S1} and T_{E1} are the self- and cross-exchange times. Then τ was obtained by fitting the signal to a single exponential and applying a small correction ($\approx10\%$) to account for the fact that the signal is only *approximately* proportional to the polarization (and hence to a single exponential). The relaxation measurement utilized rapid data accumulation with a Kerr-cell shutter and pulse-height analyzer. The cross section can be easily deduced from the relaxation times if the corresponding densities are known. Each density was measured by determining the integral over all frequencies of the absorption coefficient by means of a scanning Fabry-Perot interferometer. We describe how to remove the effect of the Fabry-Perot on the true emission and absorption profiles.

I. INTRODUCTION

THE spin-exchange process has been of particular interest during the last decade because of its importance in astronomy[1] and atomic spectroscopy.[2–6] But it is the study of interatomic potentials that motivates precise determinations of spin-exchange cross sections.[7,8] We describe such a determination of the total spin-exchange cross sections of Rb^{87}-Rb^{87} and Rb^{87}-Cs^{133} by a transient experiment involving hyperfine optical pumping. During our research, several other measurements were reported for the rubidium cross sections.[9–12] Reference 13 points out that Jarrett's neglect of nuclear spin in his analysis[10] is justified only if the relaxation is dominated by electron randomization. That such was the case was not demonstrated by Jarrett, but it was made plausible in Ref. 13 and now appears likely by the agreement between his value and ours. Also until recently the result of Davidovits and Knable[11] appeared to be less than half of the values reported by Jarrett[10] and by Moos and Sands.[9] However, Davidovits has informed us that his definition of the cross section is half ours. Our measurement of the Rb spin-exchange cross section is then in good agreement with these previous measurements and adds weight to them by serving as a cross check achieved by a different method.

Our experiment very nearly minimizes the number of subsidiary parameters that must be measured to deduce the cross section. Only three are required: the total relaxation time, the non-spin-exchange relaxation time, and the density. These quantities were measured as follows: For hyperfine pumping, the difference in populations of the hyperfine levels decays as a single exponential. This is to be compared with the sum of two exponentials for the relaxation of the longitudinal electronic polarization in a Zeeman optical-pumping transient experiment.[13] For low absorption or polarization, the Franzen[14] transient signal for hyperfine pumping is directly proportional to the hyperfine polarization. For most practical values of the absorption and polarization, corrections (as large as 12% in this experiment) must be made to account for the difference between the relaxation time deduced from the signal and that characterizing the decay of the polarization. Corresponding to each total relaxation time τ, a density measurement is made with a scanning Fabry-Perot interferometer. The analysis involves a recovery of the true emission and absorption profiles by removing the effects of the Fabry-Perot from the experimental profiles. The integral over all frequencies of the absorption coefficient, which is proportional to the density n, is then found easily. The cross section is then proportional to the slope of a plot of $1/\tau$ versus n; the intercept for $n=0$ is $1/T$ where T is the non-spin-exchange relaxation time. Observed values of T are in good agreement with values calculated with the assumption that effusion to and from the sidearms dominates the relaxation.

* Work supported by the Office of Naval Research, the U. S. Atomic Energy Commission, and the National Science Foundation.

† Present address: Physics Department, State University of New York at Buffalo, Buffalo, New York.

[1] E. M. Purcell and G. B. Field, Astrophys. J. **124**, 542 (1956).
[2] J. P. Wittke and R. H. Dicke, Phys. Rev. **103**, 620 (1956).
[3] H. G. Dehmelt, Phys. Rev. **109**, 381 (1958).
[4] L. W. Anderson, F. M. Pipkin, and J. C. Baird, Jr., Phys. Rev. Letters **1**, 229 (1958); Phys. Rev. **120**, 1279 (1960).
[5] L. W. Anderson, F. M. Pipkin, and J. C. Baird, Jr., Phys. Rev. **116**, 87 (1959).
[6] R. H. Lambert and F. M. Pipkin, Phys. Rev. **128**, 198 (1962).
[7] A. E. Glassgold and S. A. Lebedeff, Ann. Phys. (N.Y.) **28**, 181 (1964).
[8] S. A. Lebedeff, J. Chem. Phys. **40**, 2716 (1964).
[9] H. W. Moos and R. H. Sands, Phys. Rev. **135**, A591 (1964).
[10] S. M. Jarrett, Phys. Rev. **133**, A111 (1964).
[11] P. Davidovits and N. Knable, Bull. Am. Phys. Soc. **8**, 352 (1963).
[12] M. Bouchiat and J. Brossel, Compt. Rend. **257**, 2825 (1963); Phys. Rev. **147**, 47 (1966).
[13] H. Gibbs, Phys. Rev. **139**, A1374 (1965).
[14] W. Franzen, Phys. Rev. **115**, 850 (1959).

Our experiment differs from the similar one of Bouchiat and Brossel[12] in two fundamental ways. First, in our experiment circularly polarized pumping light was used instead of unpolarized light, and a resonant rf field was applied to the pumped species to destroy the resulting longitudinal polarization. This technique was necessary because it is difficult to destroy the polarization produced by the Kerr cell shutter. Second, our density measurements were made directly rather than estimated from vapor-pressure curves.

The experiment is described briefly in Sec. II, the experimental procedure in III, and the apparatus in IV. Data analysis is discussed in Sec. V, and Sec. VI is a summary of the results. For a more detailed discussion of parts of this research see Ref. 15. However, the density-measurement analysis presented here supersedes the simpler approach of that reference. Also corrections for optical thickness discussed in Sec. V were not applied to the relaxation-time data in Ref. 15.

II. DESCRIPTION OF THE EXPERIMENT

Alkali spin-exchange cross sections can be measured by a transient hyperfine-optical-pumping experiment as follows. A large difference between the ground-state hyperfine populations is achieved by irradiating the resonance cell with light that can be absorbed by only one of the hyperfine levels. The relaxation of this population difference can be observed by Franzen's method[14] of monitoring the transmitted light. If $A(t)$ is the absorption by the resonance cell at time t, a signal can be defined as

$$S=[A(\infty)-A(t)]/[A(\infty)-A(0)]. \quad (1)$$

If the absorption is not too high (see Sec. V), the approximate signal is

$$S_A=[p_+(t)-p_+(\infty)]/[p_+(0)-p_+(\infty)]=\exp(-t/\tau), \quad (2)$$

with

$$1/\tau=1/T_1'+1/T_1''+1/T_{E1}+1/T_{S1},$$

where $p_+(t)$ is the density of atoms in the $F_1=I_1+\frac{1}{2}$ hyperfine level at time t, T_1' and T_1'' are the electron randomization and uniform ground-state relaxation times, T_{E1} is the characteristic time for spin-exchange collisions between nonidentical atoms (cross exchange), and T_{S1} is the characteristic time for spin-exchange between identical atoms (self exchange). In most practical cases, (2) is not strictly valid and one must correct for optical thickness of the cell (see the Appendix and Sec. VA).

The spin-exchange cross sections are related to the values of τ as follows. The self-exchange time is defined as

$$1/T_{S1}=B_{S1}p=p\int\int |f_t-f_s|_{S1}^2 d\Omega\, v_{S1} f(v_{S1}) d^3v_{S1}/4, \quad (3)$$

where p is the density of the pumped alkali species, f_t and f_s are the triplet and singlet scattering amplitudes, respectively, for self-spin exchange, v_{S1} is the relative velocity between atoms of the pumped species, and $f(v_{S1})$ is the distribution of relative velocities. In a completely analogous manner, $1/T_{E1}$ equals $B_{E1}d$, where d is the density of the second (disoriented) alkali species. If the relative velocities obey a Maxwell-Boltzmann distribution, and if $\int |f_t-f_s|^2 d\Omega$ is assumed to be approximately independent of energy over the range of normal velocities, B_{S1} equals $\sigma_{S1}\bar{v}_{S1}$ and B_{E1} equals $\sigma_{E1}\bar{v}_{E1}$, where $\bar{v}=[8kT(1/M_1+1/M_2)/\pi]^{1/2}$ and σ is a spin-exchange cross section. Then for a single species

$$\sigma_{S1}=[\Delta(1/\tau)/\Delta p]/\bar{v}_{S1}, \quad (4)$$

assuming that $1/T_1'+1/T_1''$ is independent of the density p. For two species, $\Delta(1/\tau)/\Delta d$ equals $\sigma_{E1}\bar{v}_{E1}$ if $1/T_1'+1/T_1''+1/T_{S1}$ is independent of d and if p is held fixed. The cross sections can then be obtained if several values of $1/\tau$ and the corresponding densities are determined.

The integral over all frequencies of the true absorption coefficient $k_T(\nu)$ is proportional to the density[16]; in fact, for absorption of light emitted in the transition $J'F'M'$ to JFM,

$$\int k_T(\nu)d\nu|_{J'F'M'\to JFM}=(\lambda_0^2/8\pi\tau_{J',J})n_{JFM}(2J'+1)\sum_q\begin{pmatrix}F' & 1 & F\\ -M' & q & M\end{pmatrix}^2\times(2F+1)(2F'+1)\begin{Bmatrix}J' & F' & I\\ F & J & 1\end{Bmatrix}^2, \quad (5)$$

where λ_0 is the approximate wavelength of the emitted radiation, $\tau_{J',J}$ is the partial lifetime of the J' excited state against spontaneous radiation to the J state and n_{JFM} is the density of the JFM ground state; 3-j and 6-j symbols appear in the summation.[15] It is assumed that the excited-state density is always small compared with the ground-state density and that reradiated light can be neglected. When more than one transition is included in the integral on the left side of (5), simply sum over those transitions on the right side of (5).

Suppose that the beam of light incident upon the cell is represented by $f(\nu)$; then the transmitted light is given by

$$f(\nu)\exp[-k_T(\nu)l], \quad (6)$$

where $k_T(\nu)$ is the *true* absorption coefficient and l is

[15] H. M. Gibbs, Ph.D. thesis, University of California, Lawrence Radiation Laboratory Report No. UCRL-16034, 1965 (unpublished); H. Gibbs and R. J. Hull, Bull. Am. Phys. Soc. **10**, 704 (1965).

[16] A. C. G. Mitchell and M. W. Zemansky, *Resonance Radiation and Excited Atoms* (Cambridge University Press, Cambridge, England, 1961), p. 96.

the absorption path length. If an instrument with slit function $g(\nu-\nu')$ is used to observe the spectral profile, the incident profile appears as

$$I_0(\nu)=\int f(\nu')g(\nu-\nu')d\nu'. \quad (7)$$

Similarly, the transmitted profile becomes

$$I_0'(\nu)=\int f(\nu')\exp(-k_T(\nu')l)g(\nu-\nu')d\nu'. \quad (8)$$

The *observed* absorption coefficient is defined as

$$k_0(\nu)=l^{-1}\ln[I_0(\nu)/I_0'(\nu)]. \quad (9)$$

Clearly, if g is proportional to a delta function, $k_0(\nu)$ equals $k_T(\nu)$; for an actual instrument, there seems to be no simple relationship between the observed and true absorption coefficients. This fact is the basis for the difficulties encountered in estimating the densities by means of the Fabry-Perot profiles (see Sec. VB).

III. EXPERIMENTAL PROCEDURE

In Sec. II we showed that under proper conditions a spin-exchange cross section can be deduced from a series of measurements of the relaxation time and the density. A block diagram of the experimental apparatus is shown in Fig. 1.

A. Relaxation-Time Technique

The determination of the relaxation curve (2) by Franzen's method is demonstrated in Fig. 2. The upper left-hand trace is the transmitted light intensity after a long exposure of the cell to the pumping radiation. The light is cut off rapidly at $t=0$; the polarization relaxes in the dark according to (2). After an off interval of length t, the light is suddenly turned on again; the new level of polarization is represented by the bright spot in Fig. 2, in which the traces for many off intervals are superimposed. In most cases, data were taken for off intervals of 0, 5, 10, $\cdots$, 70 msec and 100, 125, $\cdots$, 325 msec. The relaxation of the polarization is seen more easily in Fig. 3, where the bright spots define the relaxation curve (2). As time increases after each bright spot, an optical pumping transitent occurs as the initial polarization is restored.

The data were taken at the beginning of the bright spots. To increase the precision of the measurements, several (10 to 50) relaxation curves were accumulated by a pulse-height analyzer (PHA). The PHA output was then least-squares fitted to Eq. (2) plus a constant background.

B. Density Measurement

In order to obtain the spectral profiles $I_0(\nu)$ and $I_0'(\nu)$, we used a scanning Fabry-Perot.[17] The resonance radiation of the alkali species whose density was to be determined was divided into two beams, one of

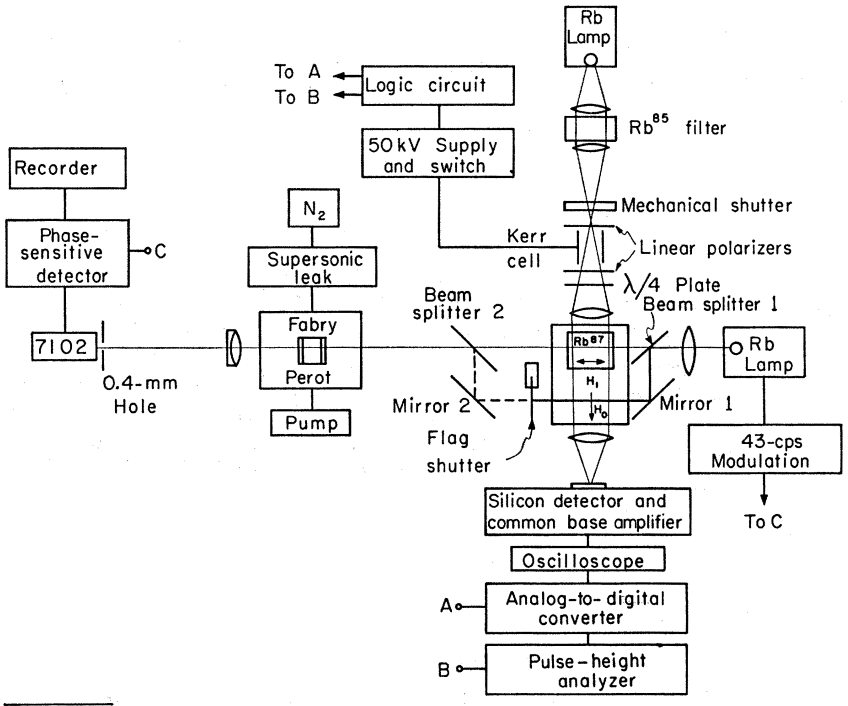

FIG. 1. Block diagram of the experimental apparatus for spin-exchange cross-section experiment by hyperfine optical pumping.

[17] P. Jacquinot, Rept. Progr. Phys. 23, 267 (1960).

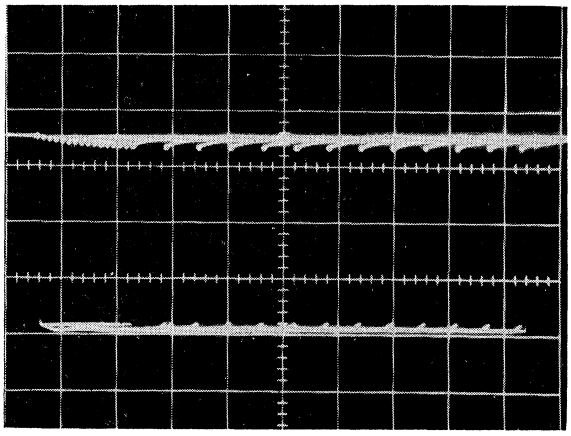

FIG. 2. Total light signal obtained with hyperfine pumping (5 mV/cm, 25 msec between long off intervals, 5 msec between short off intervals).

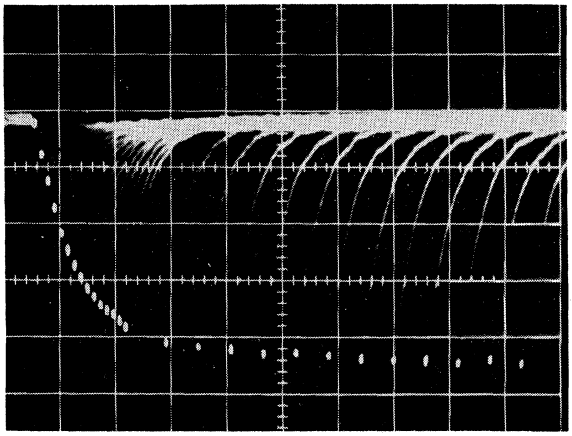

FIG. 3. The top of Fig. 2 with the vertical axis amplified 25 times (0.2 mV/cm).

which traversed the cell and the other bypassed it. With suitably placed mirrors and beam splitters, the beams were carefully brought back together and made to pass through the Fabry-Perot parallel to each other. The center spot of the ring system of each was focused on a 0.4-mm pinhole placed in front of a cooled 7102 photomultiplier. The light was electronically chopped at 43 or 86 cps in order that phase-sensitive detection could be used. The spectral profile of the radiation was traced out by scanning through several orders of the ring system. This scanning was accomplished by evacuating the chamber containing the Fabry-Perot etalon and then increasing the pressure in the chamber linearly with time by allowing dry nitrogen to pass through a supersonic "leak" (a fine capillary about 1 cm long).[18] From the equation for constructive interference in a Fabry-Perot, $2\mu t\cos\theta = m\lambda$, a change $\Delta\mu$ in index of refraction causes a change $\Delta m = 2t\Delta\mu/\lambda$ in the order number for $\theta = 0°$; t is the plate separation and λ the wavelength. From a good vacuum ($\mu \approx 1.0000$) to dry nitrogen at one atmosphere ($\mu \approx 1.0003$), $\Delta m = 7.5$ orders for $t = 10$ mm and $\lambda = 8000$ Å. With a backing pressure of 18 to 20 lb/in.^{2}, the scanning rate was linear to better than 1%.

A two-position flag shutter operating at ≈0.15 cps switched back and forth between the two beams. In the absence of absorbing atoms, the two beams were equalized so that no appreciable difference between

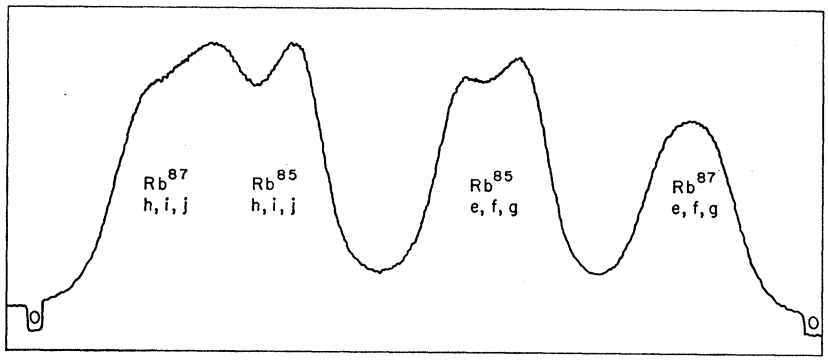

FIG. 4. Density-measurement normalization of 7800 Å line made with a natural-Rb lamp heated to help equalize the hyperfine components and broaden lines. There was no Rb in the absorption cell. The flag shutter changed position every 3 sec (chart speed 2 in./min), although it is difficult to detect it from the scan (0.3-sec integration time in the phase-sensitive detector; 12-mm spacer). The discontinuities at the far left and right are zeros of light intensity taken by inserting a flag in front of the Fabry-Perot.

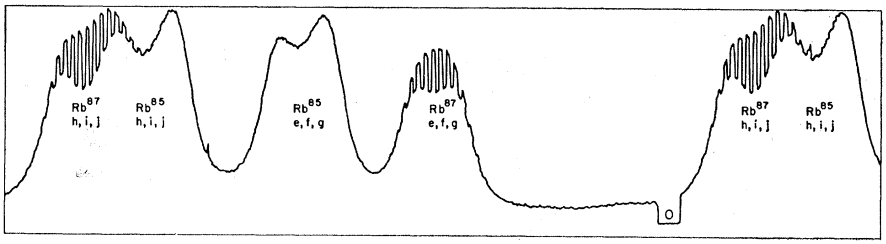

FIG. 5. Density scan showing absorption of natural Rb 7800 Å radiation by Rb^{87}. Absorption cell at 24°C, run 5. See Fig. 4 for other experimental conditions.

[18] D. H. Rank and J. N. Shearer, J. Opt. Soc. Am. 46, 463 (1956).

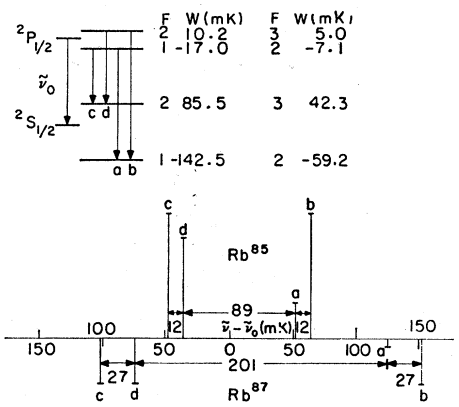

FIG. 6. Relative intensities and separations of the hyperfine-structure components of the Rb^{87} and Rb^{85} $5^2P_{1/2} \rightarrow 5^2S_{1/2}$ transitions at 7947 Å. W is the energy relative to the energy of the fine-structure level. [The $^2S_{1/2}$ energies are given by B. Bederson and V. Jaccarino, Phys. Rev. **87**, 228 (1952), and the ^2P energies by B. Senitzky and I. I. Rabi, Phys. Rev. **103**, 315 (1956).]

Transition	$\tilde{\nu}-\tilde{\nu}_0$(mK)	Rb^{87} I	f value	$\tilde{\nu}-\tilde{\nu}_0$(mK)	Rb^{85} I	f value
a	125.5	7.4	1/48	52.1	28.6	10/324
b	152.7	37.2	5/48	64.2	100.0	35/324
c	−102.5	37.2	5/48	−49.3	100.0	35/324
d	−75.3	37.2	5/48	−37.2	80.0	28/324

The relative intensities I are normalized so that the largest is 100 (a natural abundance ratio of 2.59 is assumed for the ratio of Rb^{85} to Rb^{87} densities). The f values are normalized so that their sum is $\frac{1}{3}$ for each isotope. The theoretical f values (and I) can be calculated as in Appendix IV of Ref. 15.

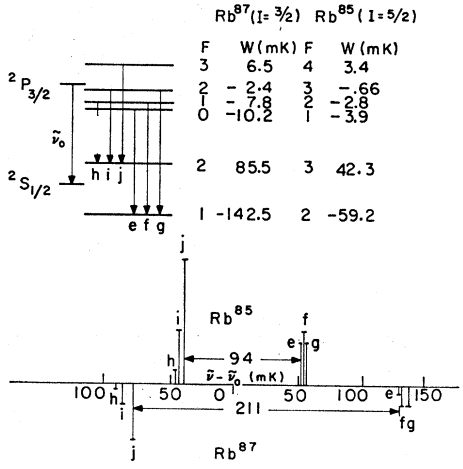

FIG. 7. Relative intensities and separations of the hyperfine-structure components of the Rb^{87} and Rb^{85} $5^2P_{3/2} \rightarrow 5^2S_{1/2}$ transitions at 7800 Å. W is the energy relative to the energy of the fine-structure level. (See Bederson and Jaccarino and Senitzky and Rabi cited above.)

Transition	$\tilde{\nu}-\tilde{\nu}_0$(mK)	Rb^{87} I	f value	$\tilde{\nu}-\tilde{\nu}_1$(mK)	Rb^{85} I	f value
e	132.3	6.4	2/48	55.3	33.4	27/324
f	134.7	16.1	5/48	56.3	43.2	35/324
g	140.1	16.1	5/48	58.5	34.6	28/324
h	−93.3	3.2	1/48	−45.1	12.3	10/324
i	−87.9	16.1	5/48	−43.0	43.2	35/324
j	−79.0	45.0	14/48	−38.9	100.0	81/324

The relative intensities I are normalized so that the largest is 100 (a natural abundance ratio of 2.59 is assumed for the ratio of Rb^{85} to Rb^{87} densities). The f values are normalized so that their sum is $\frac{2}{3}$ for each isotope. The f values (and I) can be calculated as in Appendix IV of Ref. 15.

them could be detected over a complete order; see Fig. 4. This required that the two beams pass through the same part of the Fabry-Perot because the finesse may change from one region of the plates to another.[15] In the presence of absorbing atoms, the intensity of the beam passing through the cell was, of course, diminished; see Fig. 5. The observed absorption coefficient $k_0(\nu)$ was then determined by (9).

IV. APPARATUS

A. Relaxation-Time Equipment

1. Lamp

The source of resonance radiation was a Brewer lamp[19] with a natural Rb lamp bulb. Under stable ambient conditions and with an aged bulb, the lamp noise was about 0.1% of the total light signal and the drift was usually no more than a few tenths of a percent in ten minutes.

2. Hyperfine Filter

For hyperfine pumping, radiation absorbable by atoms in the $F=2$ hyperfine level of Rb^{87} was removed by a Rb^{85} filter cell containing 6 cm of argon.[12,20,21] Figures 6 and 7 displays the energy levels for 7947 and 7800 Å transitions in Rb. The efficacy of the filter cell is demonstrated in Fig. 8 for the 7800 Å line; similar results were obtained for the 7947 Å line.[15]

3. Shutter

To avoid distortion of the signal, the light had to be cut on and off rapidly. Since the optical pumping signal was often only 1% of the total light signal and since the relaxation time was sometimes as short as 10 to 20 msec, the light should reach 99.9% of its final value in 1 msec or less. The off interval of the shutter should be easily variable from 1 msec to seconds, and the on interval should be 100 msec or longer to ensure that the equilibrium polarization be attained each cycle. The shutter should be capable of rapid cycling for thousands of cycles. Finally, an aperture with a diameter of at least 1.5 cm was needed to achieve reasonable pumping times.

A Kerr cell (Electro-Optical Instruments Model

[19] R. G. Brewer, Rev. Sci. Instr. **32**, 1356 (1961).

[20] P. Davidovits and N. Knable, Rev. Sci. Instr. **35**, 857 (1964).

[21] P. L. Bender, E. C. Beatty, and A. R. Chi, Phys. Rev. Letters **1**, 311 (1958).

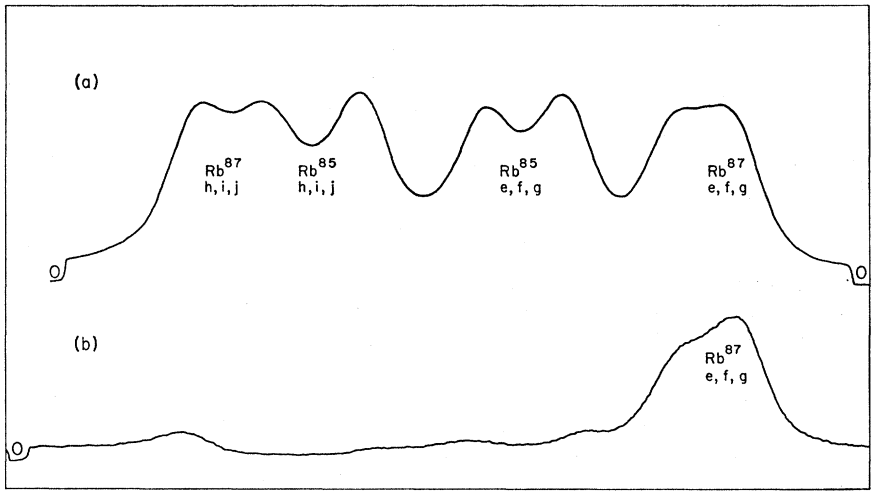

FIG. 8. Effect of Rb^{85} filter cell on the 7800 Å line from a natural-Rb lamp. The traces are in approximately the correct frequency relationship to one another. The intensities are unnormalized. (a) Without filter. (b) With filter.

K93/150P) was chosen as the shutter. The high-voltage switching circuit diagram is shown in Fig. 9. Care had to be taken to protect against the high voltage and x rays. When the switch tubes were conducting, the Kerr cell was discharged through the Zener diode that cut off the charge tubes. The Kerr cell can be charged more quickly if the charge tubes are used. Since the cathode voltages of these tubes swung from a few to many kV, the filaments were supplied by 5 4FH 1.5-V batteries. In preliminary runs for which a fast off time was unimportant, the filaments were cut off and the Zener diode shorted. The dummy-load tubes conducted when the switch tubes were off, and vice versa, to maintain a constant output voltage from the supply.

The linear polarizers of the Kerr-cell shutter were arranged to be normally transmitting, because a fast rise time was more important than a fast fall time in this experiment. The time for the light signal to fall to 10% of the initial value was about 0.5 msc. The rise time to the 90% level was less than 0.1 msec; to the 99.9% level, about 0.3 msec.

The Kerr-cell shutter then fulfilled excellently the outlined characteristics. But in the off mode, the Kerr cell did not extinguish the light completely; notice in Fig. 2 that the "zero" line underneath the closely spaced points (taken with the Kerr cell only) lies above the zero for the long off intervals (Kerr cell and mechanical shutter). An off transmission of as much as 10% occurred, but refilling the cell with hyperpure nitrobenzene reduced this to 3% or better. The lack of complete extinction may have resulted from a reduction of the electric field by ionic impurities attracted to the electrodes; there was also a 1% contribution from the failure of the crossed HN32 polarizers to eliminate all of the 7800 and 7947 Å light.

If the pumping time when the light is "off" is comparable to or shorter than the relaxation time, the relaxation curve is considerably altered by the "off" transmission. Consequently, for long off intervals an

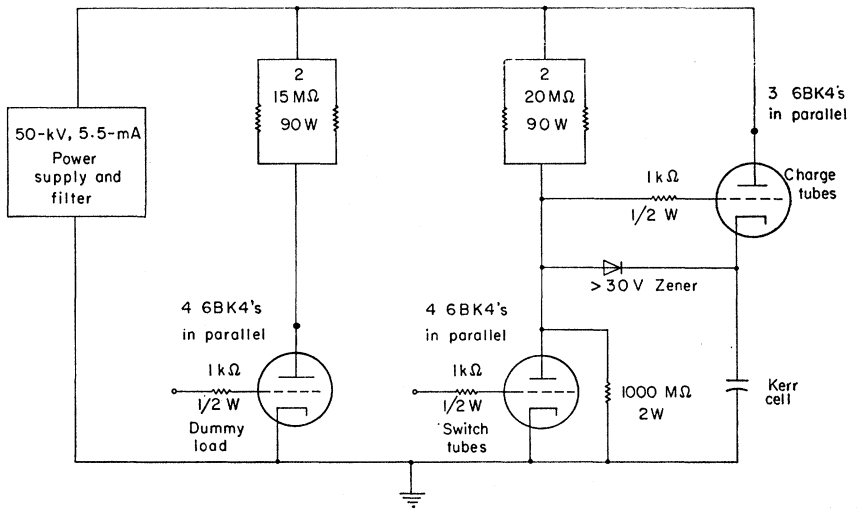

FIG. 9. The Kerr-cell-switch circuit diagram.

electrically operated mechanical shutter was synchronized with the Kerr cell. The shutter (constructed by Photographic Instrumentation Development Company, now out of business) consisted of a lightweight metallic blade, driven by a Ledex rotary solenoid and confined between two narrowly spaced surfaces with 4.5-cm-diam apertures.

4. Resonance Cell

The resonance cells were cleaned with chromic acid, evacuated to a pressure of 10^{-6} Torr or less, and baked at 350 to 400°C for 24 or more hours. Paraflint,[22] which was situated outside of the oven during the baking of the cell, was melted and allowed to run into the cool cell. After the cell was removed from the vacuum system, a thick even coating of Paraflint was achieved by heating the cell over a Bunsen burner. The cell, still under vacuum, was again baked overnight at 150–160°C; the excess Paraflint accumulated in a sidearm. The coating was tested by opening the cell and inserting a drop of water; if the coating was successful, the drop ran about freely without adhering to any point of the surface. In runs 4 to 8 a cubical cell approximately 5 cm on an edge was used. A 2.5×5×5-cm cell was used in runs 9 and 11.

Sidearms containing the desired alkali isotopes were prepared separately from the cell. Each sidearm consisted of a break-off connection and vial containing the desired metal and a sub-sidearm for the glass-enclosed ferromagnetic hammer (see Fig. 10).

After the first break-off connection was broken, an aging period of several days was necessary for good signals to appear. It was usually helpful to flame the vial gently and drive some of the metal into the sidearm and cell. Then a signal could usually be seen only with a buffer gas, i.e., the walls were probably contaminated.

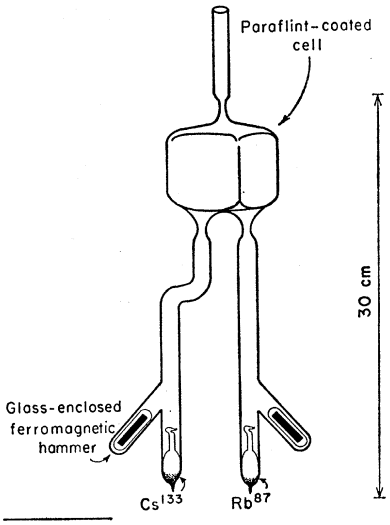

FIG. 10. Sketch of the absorption cell showing the Rb and Cs sidearms.

[22] The authors are indebted to Moore and Munger, 33 Rector Street, New York 6, New York for a generous free sample.

If the cell was then baked for several hours at 110 to 120°C, a long relaxation time was obtained. When the relaxation of the electronic longitudinal polarization achieved by pumping with circularly polarized D_1 light with equal hyperfine components (Zeeman pumping) was approximated by a single exponential, the characteristic time of various cells ranged from 140 to 500 msec. The cells were usually sealed from the vacuum system to ensure good equilibrium conditions, although good signals were observed in cells connected to the vacuum system through ≈1-mm seal offs.

The relaxation time was shortened by an extended exposure of the cell to a high density of alkalis. Although reducing the density did not restore the longer time, it could be recovered by heating the cell to between 110 and 120°C for several hours. Apparently an interaction between the alkali and impurities in the coating causes disorientation centers to form slowly. Since Paraflint melts at about 100°C, at higher temperatures the surface disorientation sites are probably lost in the huge number of coating atoms. Upon cooling there is little probability that such a site is still on the surface.

5. Detector and Amplifiers

A detector with the following properties was needed: high efficiency at 8000 Å, flat frequency response from 0 to 100 kilocycles, and linearity. Because of the slow transient response observed by Brewer,[23] S1 phototubes were avoided. A silicon photovoltaic cell, with peak sensitivity at 8000 Å was used instead. A common-base-transistor amplifier minimized the input impedance, thereby increasing the frequency response; see Fig. 11. With a 10-kΩ terminal resistance used in all the runs, the characteristic time of the detector system was 5 μsec. The linearity of the detector and amplifier were verified with the inverse-square law.

Dc coupling was used throughout to avoid distortion of the signal. The output of the common-base amplifier was fed into a Tektronix 502 oscilloscope. Since the desired signal rode on a modulated background 20 to 100 times the signal height, the bias box portion of Fig. 11 was necessary. The signals, usually observed on the 0.5 or 1 mV/cm scale, produced deflections of about 2 cm. For further amplification, the voltage of the oscilloscope plates (6 V/cm of deflection) was shifted down by 225 V and applied to a cathode follower. The output of the latter drove the analog-to-digital converter.

The detector and transistor were housed in a brass cylinder through which ice water was circulated. This arrangement prevented signal drifts arising from changes in transistor characteristics with fluctuations in room temperature. In addition, cooling helped eliminate the "sag effect." Apparently the transistor was so temperature sensitive that the change in

[23] R. G. Brewer, J. Opt. Soc. Am. **52**, 832 (1962).

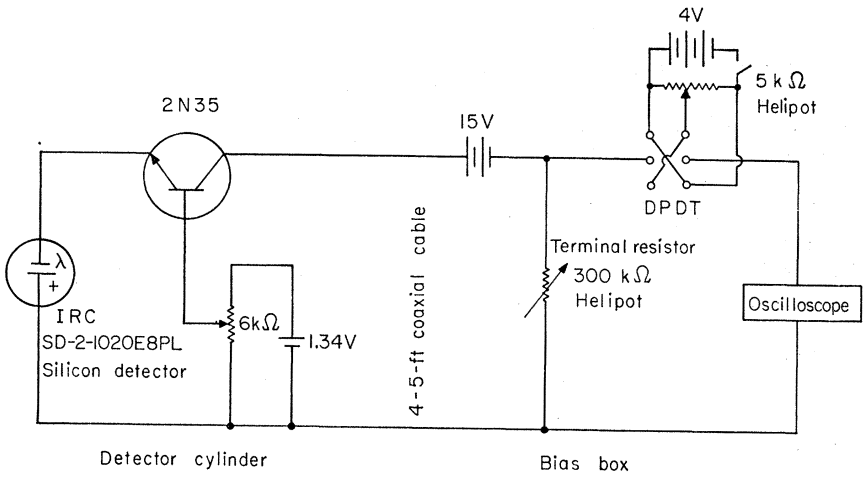

FIG. 11. Circuit diagram of the common-base amplifier and bias box.

dissipated power when the light was cut off allowed the transistor to cool sufficiently to reduce its reverse-bias saturation current. Consequently, when the light was turned on the apparent signal was smaller than initially and then gradually returned to the initial value. This gave rise to a spurious signal or sag effect as large as 0.4% of the total light—an appreciable fraction of the true signal. The characteristic time of about 5 msec is typical for thermal time constants for switching transistors. When the transistor was cooled to 0°C, the sag effect became a rise effect because the reverse-bias current was negligible and the emitter-base junction has a negative temperature coefficient of resistance. Thus when the illumination was suddenly increased the transistor was heated; the temperature increase caused a decrease in the emitter-base voltage, which in turn reduced the collector current and output. But if an emitter-base forward bias was applied, the temperature-induced changes in the saturation current became significant at lower temperatures. The sag effect was reduced to less than 0.02% of the total light by cooling the detector system and adjusting the forward bias to eliminate the rise effect.[15]

6. *Logic Circuit and Pulse-Height Analyzer*

In order to improve the precision of the measurements, the relaxation curve was traced out many times and the data stored in a pulse-height analyzer (PHA). An elaborate logic circuit furnished the command pulses for the Kerr cell switch, mechanical shutter, analog-to-digital converter (ADC), and PHA.[15] A stretcher in the ADC maintained a voltage at the level of the signal from the oscilloscope at the time of the take-data pulse (beginning of bright spot) until a train of 500 kc/sec pulses, whose length was proportional to the voltage height, was transmitted to the data register of the PHA. A channel of the PHA was assigned to each off interval; the address, read, and write scalers were pulsed by the logic circuit.

7. *Miscellaneous*

The ovens for the resonance cell and sidearms were constructed of $\frac{3}{4}$-in. Maronite and brass screws. Heating of the cell oven by air blown through several turns of copper tubing in another oven resulted in extreme temperature gradients of 10°C, as measured by four mercury thermometers situated around the cell.

To minimize lamp and electronic drifts, the room temperature was maintained constant.

A magnetic field of 5 to 10 G was supplied by 50-cm-diam Helmholtz coils.

The rf fields were produced by coils about 7 cm in diameter, situated inside the oven. A Tektronix 190B signal generator and a Lab-made rf oscillator drove the coils.

B. Density-Measurement Apparatus

1. *Electronics*

The lamp was driven by a 25-Mc/sec multivibrator,[24] screen-grid modulated at 43 or 86 cps; 2.5 to 3 cm Pyrex bulbs containing 1 mm of argon and the alkali metal were used. The bulb and coil were housed in an aluminum box equipped with a small heater for regulating the self-reversal and relative intensities of the hyperfine components.

The detector was a cooled photomultiplier (RCA 7102) operated at 1200 V. A lock-in amplifier designed and constructed by Al George and the Department's Electronics Shop was used. The time constant of the lock-in amplifier was usually set at 0.3 sec—one-tenth of the time the flag shutter was in each of its positions.

The flag shutter was driven by a Leland two-position stepper or solenoid, powered by about 10 V dc at 1 A and switched by an ≈0.15-cps multivibrator and Hg switch.

[24] C. O. Alley, Princeton University Report, 1960, p. III-11 (unpublished).

2. Optics

The mirrors were front-surface silver coated; the beam splitters were approximately 50% transmitting. Because the focusing lens (36-cm focal length) was an achromat, the ring system could be focused for the infrared with visible light.

Filters eliminated undesired lines. A trimmer filter eliminated light above 12000 Å and below 7000 Å. Narrow-band ($\approx$80 Å) interference filters (from Spectrolab) passed the D line of interest. A Kodak Wratten filter 87C eliminated stray lines that passed through the Spectrolab 8944 Å filter for Cs.

The Fabry-Perot plates, obtained from Aurora Precision Optics, were quoted to be flat to $\lambda/200$ in the green. They were silver coated by Dan O'Connell, Lawrence Radiation Laboratory, so that they transmitted 5% of the light at 8000 Å. The spacers (built by the U. C. Physics Department Shop) consisted of Invar pins housed in aluminum rings and were accurate to $\lambda/4$. A 12-mm spacer was used for the Rb scans and 10 mm for the Cs scans.

The etalon was enclosed by a brass cylindrical vacuum chamber about 15 cm in diameter and 25 cm in length. To minimize distortion of the ring system, the exit window of the chamber was flat to $\lambda/4$. The screws for adjusting the parallelism of the plates were controlled by extensions which reached the outside of the chamber through O-ring seals. The chamber rested on a mount that could be rotated about both vertical and horizontal axes. A Duo-Seal forepump evacuated the chamber.

V. DATA ANALYSIS

A. Relaxation-Time Data

1. Extraction of Relaxation Time by Least-Squares Fit

The data from the pulse-height analyzer were punched onto cards and least-squares fitted (after being normalized to unity for time $t=0$) by an IBM 7090 computer to the theoretical curve

$$F(t)=A\exp(-t/\tau)+C; \tag{10}$$

see Eq. (2). Figure 12 contains data at three different temperatures chosen at random from run 7. The points shown there are proportional to the normalized data points $S(t)$ less the best-fit background C, i.e., $[S(t)-C]/(1-C)$, where the division by $(1-C)$ renormalizes the new signal to unity at $t=0$. The straight lines are the best-fit curves $[F(t)-C)]/(1-C)$.

In order to be completely explicit in the area of data handling, a brief summary of the formulas will now be given. The quantity

$$Q=\sum_{i=1}^{n} W_i[S(t_i)-F(t_i,b_k)]^2 \tag{11}$$

was minimized. The W_i, the weights of the n data points, were taken to be equal. The b_k are the parameters

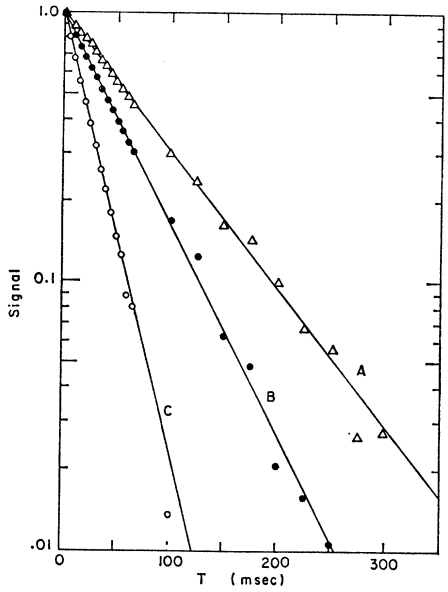

FIG. 12. Relaxation-time data chosen at random from run 7; each is comprised of 20 accumulation cycles. The straight lines are the least-squares best fits. Curve A: $T_{Rb^{87}}=24$°C, $1/\tau=11.89\pm0.18$ sec^{-1}; B, 30° (18.12±0.28); C, 38° (38.12±0.37).

A, C, and τ in (10), $k=1, 2, \cdots, p$. Minimization leads to the set of equations

$$\sum_{k=1}^{p}\Delta(k)P(k,j)=Q(j), \tag{12}$$

where

$$P(k,j)=\sum_{i=1}^{n} W_i[\partial F(t_i)/\partial b_k][\partial F(t_i)/\partial b_j], \tag{13}$$

$$Q(j)=\sum_{i=1}^{n} W_i[\partial F(t_i)/\partial b_j][S(t_i)-F(t_i)], \tag{14}$$

and $\Delta(k)$ is the calculated estimate of the correction to be applied to b_k to minimize Q:

$$b_k \rightarrow b_k+\Delta(k). \tag{15}$$

The quantities involving $F(t_i)$ in (13) and (14) were evaluated at the trial values. The $\Delta(k)$ were found by inverting P; the new trial values were placed in (13) and (14) and new corrections calculated. This process was continued until the correction for each parameter was less than 10^{-4} of the value of the parameter. In the program used, only 25% of the correction was applied each cycle; approximately 20 to 25 iterations were normally required to satisfy the convergence criterion.

Since the weights were assigned arbitrarily, the only meaningful standard deviation was that of external consistency, i.e., of how well the points fitted the assumed form of the curve. These standard deviations were calculated by

$$\sigma(k)=[VP^{-1}(k,k)]^{1/2}, \tag{16}$$

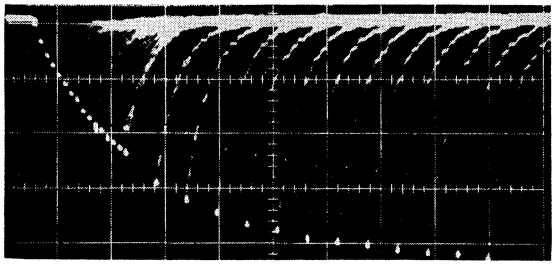

FIG. 13. Typical hyperfine pumping and relaxation transients in Rb^{87}. Absorption cell at 24°C, run 5.

where the weighted variance is

$$V=\sum_{i=1}^{n} W_i[S(t_i)-F(t_i)]^2/D; \quad (17)$$

the number of degrees of freedom D is equal to the number of data points n minus the number of parameters p. The standard deviations of $1/\tau$ rarely ranged outside of 0.5 to 2% of $1/\tau$; $\sigma(A)\approx 0.005\ A$, $\sigma(C)\approx 0.001\ C$.

2. Cell-Length Correction to the Relaxation Time

As was previously noted, Eq. (2) is valid only if the product of the polarization $P_{F_1}(t)=[p_{F_1}(t)-p_{F_1}(\infty)]/p_{F_1}(\infty)$ and the optical thickness $k_T(\nu)l$ is sufficiently small. In the first analysis, Eq. (2) was assumed to be valid, and the values of $1/\tau$ were found by least-squares fitting as described above. However, errors in $1/\tau$ as large as 12% were made by that procedure, as shown below. We compare here the true observed signal $S(t)$ of (A12) with the approximate signal $S_A(t)$ of (A13). From (A16), we know that

$$P_+(t)/P_+(0)=P_-(t)/P_-(0)=\exp(-t/\tau)=S_A(t). \quad (18)$$

To find $S(t)$ one must know $k_T(\nu)|_{F_1J_1'}$, $L_{F_1J_1'}(\nu,0)$, and $P_{F_1}(0)$. The absorption coefficients are known accurately: relative intensities from calculations, separations from resonance measurements, and spectral distribution from the Doppler distribution since the densities are low. The quantity $L_{F_1J_1'}(\nu,0)$ depends upon the particular conditions in the lamp. In this experiment the $F_1=I_1-\frac{1}{2}$ components were negligible compared with those for $F_1=I_1+\frac{1}{2}$. Also the $F_1=I_1+\frac{1}{2}$ components were about twice as broad as the Doppler width and were very nearly constant over the region in which the absorption was appreciable. Therefore, the details were unimportant, and a good approximation to the true spectral distribution was made from Fabry-Perot profiles.

Finally one must know $P_+(0)$ to obtain $S(t)$. The effect of the light on the density p_+ can be represented by a pumping time τ_p, so that (A16) becomes

$$\dot{p}_+(t')=\frac{-[p_+(t')-(2I_1+2)p/2(2I_1+1)]}{\tau-p_+(t')/\tau_p}. \quad (19)$$

Here $t'=0$ marks the start of the pumping process; for $t=0$, $t'=\infty$, i.e., $t'\gg\tau\tau_p/(\tau+\tau_p)$. Then at

$$p_+(t'=\infty)=p_+(t=0)=(2I_1+2)p/[2(2I_1+1)(1+\tau/\tau_p)]$$
$$=p_+(t=\infty)/(1+\tau/\tau_p) \quad (20)$$

or

$$P_+(0)=-1/(1+\tau_p/\tau). \quad (21)$$

Or solving (19) for the pumping transient, we get

$$P_+(t')=P_+(0)\{1-\exp[-(1/\tau+1/\tau_p)t']\}, \quad (22)$$

where $P_+(0)$ is the same quantity as before [although $P_+(t'=0)=0$ in (22)]. Then by observing the pumping and relaxation transients for the same conditions, we can find τ_p (neglecting the small optical-thickness correction). For an example, see Fig. 13, which was taken the same afternoon and under the same conditions as Fig. 5. Unlike the atypical curve of Fig. 3, Fig. 13 was taken under normal operating conditions in the middle of a run. From it one can deduce $\tau_p\approx 24$ msec. Since the lamp output and the signal did not vary appreciably from one run to the next, it is reasonable to assume that this value was approximately correct for all the runs. (The maximum increase of τ_p arising from a reduction of light by absorption is calculated to be 25% over the range of densities used.) The polarization can then be estimated using the $1/\tau$ from the least-squares fit in (21).

As a cross check of the above estimate of the polarization, the following comparison was made. Three levels of transmitted light intensity were easily observed with the silicon detector: the zero level, the levels corresponding to no polarization $T(\infty)$, and that corresponding to the initial polarization $T(0)$. The T's were measured relative to the zero level. One can define a signal as

$$S'=[T(0)-T(\infty)]/T(0). \quad (23)$$

In the notation of the Appendix

$$S'=\frac{\sum_{F_1J_1'}\int L_{F_1J_1'}(\nu,0)\exp[-k_T(\nu)|_{F_1J_1'}l]\{1-\exp[-P_{F_1}(0)k_T(\nu)|_{F_1J_1'}l]\}d\nu}{\int L(\nu,0)\exp\{-[1+P_{F_1}(0)]k_T(\nu)|_{F_1J_1'}l\}d\nu}. \quad (24)$$

In the denominator of (24), the nomenclature $\sum_{F_1J_1'}\times\int L_{F_1J_1'}(\nu,0)$ is replaced by $\int L(\nu,0)$ since the integral is no longer broken up nicely into parts by the vanishing of the integrand for $k_T(\nu)l\approx 0$. Notice that if there is a large contribution to $L(\nu,0)$ from background light [i.e., at frequencies for which $k_T(\nu)l\approx 0$], then S' may

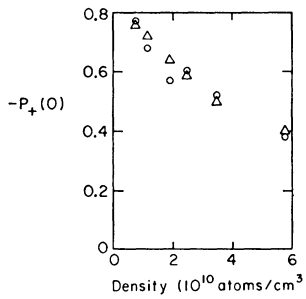

FIG. 14. Polarization of the $F_1=I_1+\frac{1}{2}$ level in Rb^{87} as a function of density. ○, values of the polarization required to make the experimental and theoretical values of S' [Eq. (24)] agree; △, values calculated from Eq. (21) with $\tau_p=24$ msec. This curve depends strongly upon the particular conditions of this experiment and therefore has no general validity—see the text.

be quite small even though $P_{F_1}(t)k_T(\nu)|_{F_1}{}^{J_1'}l$ may be appreciable. In other words, even though the apparent signal S' may be small, S may still differ appreciably from S_A. The cross check consisted of the following. The value of S' for the conditions of Fig. 13 was about 0.039. To calculate S' one needs $P_+(t)$ and details about the light intensity. We calculated $P_+(0)$ to be -0.77 using (21). The $F_1=I_1-\frac{1}{2}$ components of L were set equal to zero, and the efg component of the true emission profile of Fig. 19 taken for $L_+{}^{3/2}(\nu,0)$. The same profile scaled down by 0.667 was taken for $L_+{}^{1/2}(\nu,0)$. (The theoretical scale factor is 0.5 without self-reversal

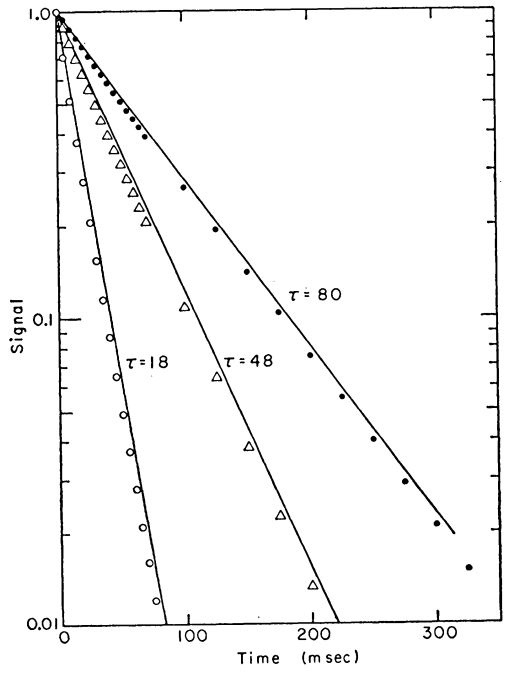

FIG. 15. Comparison of the approximate hyperfine-relaxation signals [given by (A13) and shown as the solid lines] which are single exponentials and the predicted signals [given by (A12) and represented by the points above] which are more complicated functions of the time. These curves depend strongly upon the particular conditions of the experiment.

which makes the experimental value higher. The corrections calculated here are affected only slightly by changing the ratio to 0.5 or 1.0). The theoretical S' was found to agree with the experimental value, provided that

$$\int_{-\infty}^{\infty} L(\nu,0)d\nu = 2.4\sum_{J_1'}\int L_+{}^{J_1'}(\nu,0)d\nu,$$

i.e., that the total light intensity reaching the detector was 2.4 times the light absorbable by the $F_1=I_1+\frac{1}{2}$ hyperfine level. This value is in good agreement with experimental estimates. The comparison was carried further. Keeping $L(\nu,0)$ and $L_{F_1}{}^{J_1'}(\nu,0)$ fixed, the theoretical values of S' were forced to agree with the corresponding experimental values at several densities by varying $P_+(0)$. These values of $P_+(0)$ agree to within 10% with those calculated from (21) (Fig. 14).

With good estimates of $P_+(0)$ at various densities, one can now compare $S_A'(t)$ of Eq. (18) with $S(t)$

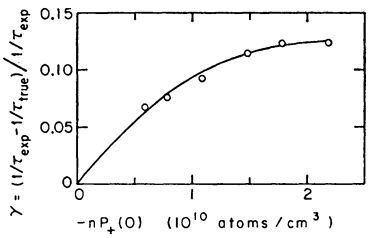

FIG. 16. Corrections necessary to deduce τ_{true}, the characteristic time of the polarization which decays as a single exponential, from τ_{exp}, the decay time obtained by fitting Eq. (A12) to a single exponential plus a constant. The corrections are plotted as a function of the product of the density and the polarization in the $F_1=I_1+\frac{1}{2}$ hyperfine level. This curve depends strongly upon the particular conditions of the experiment.

given by (A12). The light profile used in (24) was again employed. The $P_+(0)$ required to make the theoretical and experimental values of S' agree were also utilized. The values of $S(t)$ were then generated for $t=0$, 5, ···, 70 and 100, 125, ···, 325 msec for which the experimental data were taken. The resulting points were least-squares fitted just as were the actual data (Fig. 15). The value of $1/\tau$ deduced from $S(t)$—let us call it $1/\tau_{exp}$—was compared to the true value $1/\tau_{true}$ which characterized the decay of $S_A(t)$:

$$\gamma=(1/\tau_{exp}-1/\tau_{true})/1/\tau_{exp}. \qquad (25)$$

Figure 16 is a plot of γ versus the product of the density and the polarization. Notice that in this experiment, errors as large as 12% would result if the cell-length corrections were not made. Note that, in general, the corrections depend upon the length of the cell (≈ 5 cm in all the runs here) as well as the density. They depend also upon the details of $k_T(\nu)$—always $k_T(\nu)$ of Rb^{87} in this experiment—and $L(\nu,0)$ (although

insensitively if $L(\nu,0)$ changes little over the absorption frequencies).

B. Density-Measurement Data

The lock-in amplifier output was continuously recorded on a linear chart recorder. Smooth curves defined by the shutter positions were penciled in; the zero was drawn by using the zeros obtained with a flag shutter during the scan. Points 0.1 in. apart were marked along the zero line. The values of the zero, $I_0'(\nu)$, and $I_0(\nu)$ were measured at each of the marks. An ingenious machine constructed by Professor John Reynolds's group was used; with this machine, one set a crosshair on the point, pressed a button, and waited a second for the coordinates to be punched onto an IBM card. A computer program computed $k_0(\nu)l$ and $\int k_0(\nu)ldv$.

In Sec. II we noted that the integral over all frequencies of the true absorption coefficient is proportional to the density. The problem is then to obtain that integral from the experimental data. Kostkowski and Bass[25] showed that the integral of the observed coefficient is approximately equal to the integral of the true coefficient even when the observed and true peak coefficients are greatly different. But their calculations were made for a Gaussian instrument function. Prompted by early results of our experiment, Hull and Bradley studied the effects of the Airy function.[26] They reported that the true and observed integrals can differ appreciably, primarily because the Airy function has nonnegligible values compared to a Gaussian throughout the between peak region. Consequently, absorption occurring at one frequency is observed to some extent at all frequencies, causing the observed integral to be too high. The Airy function can also reduce the coefficient if there is a nearby unabsorbable component in the incident light. For example in Fig. 5, the Airy function effectively caused some of the Rb^{85} *hij* light to be observed at the frequencies of the Rb^{87} *hij* absorption. This effect increased the observed values of $I_0(\nu)$ and $I_0'(\nu)$, Eqs. (7) and (8), and thereby reduced $k_0(\nu)$. These two distortions introduced by the Airy function were ignored in Ref. 15. By accident, the two effects were both about 10% and in opposite directions; thus our deduced values of the cross section were affected very little.

Then if the instrument function is an Airy function, the observed absorption coefficient and its integral over all frequencies depend strongly on the spectral distribution of the incident radiation and upon neighboring absorption lines. Clearly, one would like to remove entirely the effect of the instrument and regain the true absorption coefficient. This we did do; our method

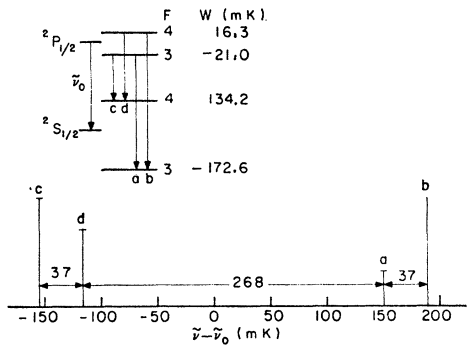

FIG. 17. Relative intensities and separations of hyperfine-structure components of the $Cs^{133}(I=\frac{7}{2})6^2P_{1/2} \rightarrow 6^2S_{1/2}$ transition at 8944 Å. W is the energy relative to the energy of the fine-structure level. [The $^2S_{1/2}$ hyperfine-structure separation is given by L. Essen and J. V. L. Parry, Nature **176**, 280 (1955), and the $^2P_{1/2}$ by Landolt-Börnstein, *Zahlenwerte and Funktionen* (Springer-Verlag, Berlin, 1952), I Band, 5 Teil Atomkerne, p. 37.]

Transition	$\tilde{\nu}-\tilde{\nu}_0$(mK)	I	f value
a	150.7	33.4	7/192
b	189.6	100.0	21/192
c	−156.1	100.0	21/192
d	−117.2	71.5	15/192

The relative intensities I are normalized so that the largest is 100. The f values are normalized so that their sum is $\frac{1}{3}$ for the $^2P_{1/2} \rightarrow {}^2S_{1/2}$ transition.

is described after a more explicit relation between the density and integral of $k_T(\nu)$ is presented.

From Eq. (5) for the $^2P_{3/2}$ to $^2S_{1/2}$, $F=1$ transition in Rb^{87} (see Figs. 6 and 7), $\lambda_0=7800$ Å, $I=\frac{3}{2}$, and[27] $\tau=(2.78\pm0.09)\times10^{-8}$ sec, one finds

$$n_{Rb^{87}}=(1.8\times10^{12})\frac{1}{l}\int k_T(\nu)ldv|_{7800\text{ Å},\,efg}\ \text{cm}^{-3} \quad (26)$$

with the integral in cm^{-1}. For the $^2P_{1/2}$, F' to $^2S_{1/2}$, F transition in Cs^{133} (see Fig. 17), $\lambda_0=8944$ Å, $I=\frac{7}{2}$, and[28] $\tau=(3.12\pm0.03)\times10^{-8}$ sec

$$n_{Cs}=(5.56\times10^{13}/\Delta(F,F'))\times\frac{1}{l}\int k_T(\nu)ldv|_{8944\text{ Å},\,F'\rightarrow F}\ \text{cm}^{-3}, \quad (27)$$

where

$$\Delta(F,F')=6(2F_1+1)(2F_1'+1)\begin{Bmatrix}\frac{1}{2} & F' & I_1\\ F & \frac{1}{2} & 1\end{Bmatrix}^2$$

are given in Table II of Ref. 13.

For a single Gaussian with peak $k_T(\nu_0)$, one has[29]

$$\int k(\tilde{\nu})ld\tilde{\nu}=(\pi)^{1/2}k_T(\tilde{\nu}_0)l\Delta\tilde{\nu}_a/2(\ln2)^{1/2}, \quad (28)$$

[25] H. J. Kostkowski and A. M. Bass, J. Opt. Soc. Am. **46**, 1060 (1956).

[26] R. J. Hull and L. C. Bradley, III, J. Opt. Soc. Am. (to be published).

[27] G. Stephenson, Proc. Phys. Soc. (London) **A64**, 458 (1951). The theoretical value, determined by O. S. Heavens, J. Opt. Soc. Am. **51**, 1058 (1961), is 26.7 nsec.

[28] The original references are given in M. Rozwadowski and E. Lipworth, J. Chem. Phys. **43**, 2347 (1965). Heavens's theoretical value (see Ref. 27) is 35 nsec.

[29] Reference 16, p. 99.

where

$$\Delta\tilde{\nu}_a = 2(2kT\ln 2/M)^{1/2}\tilde{\nu}_0/c \qquad (29)$$

is 18.4 mK (10^{-3} cm^{-1}) for the 7800 Å line of Rb^{87} and 13 mK for the Cs 8944 Å line at $T=78$°C, the temperature of the oven in all the runs. If several Gaussian absorption lines of known relative intensities are present, one can find $k(\nu)$ by summing the component coefficients at each frequency. (In this experiment, performed with no buffer gas and with low vapor densities, the absorption profiles were dominated by Doppler broadening.) Therefore the integral of $k_T(\nu)$, consisting of several Gaussians, is a constant times any one of the component peaks. Hence the true coefficient for only one of the components (with thermal equilibrium assumed) need be found to determine the density.

The technique can be summarized briefly. (1) Find an instrument function agreeing with various experimental data. (2) Obtain a "true" emission function whose convolution with the instrument function reproduces the observed emission profile. (3) Generate $k_T(\nu)$ by summing Gaussians of the proper width, separations, and relative intensities, and adjust the over-all scale factor so that the difference between the predicted absorption profile and the observed absorption profile is minimized. (4) From $k_T(\nu)$ and Eqs. (26) and (27), find the density for the model case (corresponding to a particular observed peak-absorption coefficient times the cell length, such as the *efg* peak in Rb^{87}—see Fig. 5). Obtain corrections for other observed peak coefficients by repeating the calculations of $\int k_T(\nu)d\nu$ and $k_0(\nu_0)$ for other over-all scale factors.

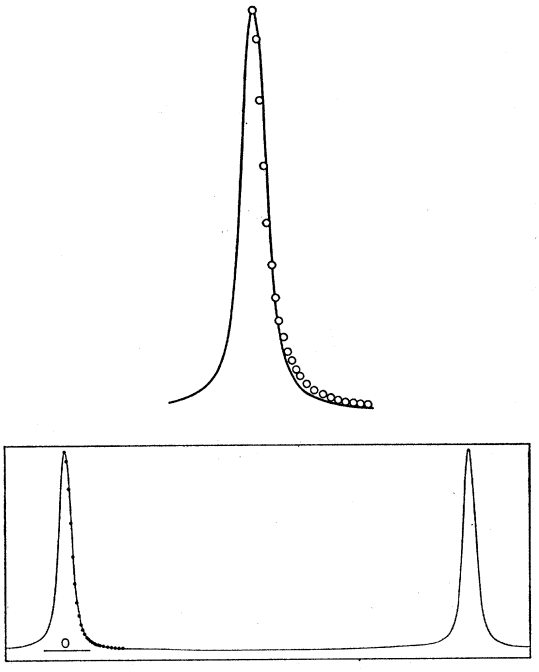

FIG. 18. The solid curves are experimental instrument profiles taken with a monochromator to isolate the 8115 Å line of argon. The points represent a convolution of Airy function ($R=0.935$) with Gauss function (width 9.5 mK for free spectral range, $F_\sigma=420$ mK, i.e., finesse $N=44.0$). Above: The open circles correspond to an Airy function with reflection coefficient $R=0.893$.

1. Fabry-Perot Instrument Function

In order to remove the effect of the Fabry Perot, the instrument function must be known. The experimental instrument function was found using a 1.5-mm spacer and a narrow line (≈35 mK) of argon. The effect (≈10%) of the width of the argon line was removed with the formulas of Minkowski and Bruck.[30] The finesse (defined as $N=F_\sigma/\Delta\sigma$, where $F_\sigma=1/2t$ is the free spectral range, t is the spacer thickness, and $\Delta\sigma$ is the width of the instrument function at half maximum) was then determined. For the experimental instrument function presented in Fig. 18, the observed finesse was about 28 and the corrected "true" finesse about 31.

One might be tempted to assume that the Fabry-Perot function is an Airy function with an effective reflection coefficient reduced below the measured value to account for nonflatness, etc.[15] However, the latter effect is better represented by a Gaussian distribution as evidenced by Fig. 18.[31] The figure demonstrates that the observed instrument function was reproduced excellently by the convolution of Gauss and Airy functions of the proper widths. An Airy function alone, with a width equal to the observed width, was a poor fit. The need for the Gauss portion was also demonstrated by the fact that the Airy function alone predicted too much absorption for frequencies somewhat removed from absorption peaks. Calculations using the Airy function alone also predicted an absorption coefficient width larger than the observed value. When the proper instrument function is chosen, the predictions agree well with the observations.

Limits of about 2% were placed on the possible values of the reflection coefficient by measuring the transmission of the Fabry-Perot plates with a Beckman spectrophotometer and estimating the absorption of Ag films according to the measurements of Kuhn *et al.*[32] The limits ranged from 0.92 to 0.955. Good agreement between the observed instrument function and absorption data were obtained with values within these limits. Furthermore the density was changed only a few percent by changes within each set of limits.

2. True Emission Profile

A straightforward but involved procedure of trial, error, and simple feedback was used to find a function which, when convolved with the instrument function, reproduced the observed emission profile. The feedback consisted of simply incrementing the trial function at

[30] R. Minkowski and H. Bruck, Z. Physik **95**, 299 (1935).
[31] R. Chabbal, (thèse), University of Paris, 1957; also Rev. Opt. **37**, 49, 336, 501 (1958). (Also see Ref. 17).
[32] H. G. Kuhn and J. M. Vaughan, Proc. Roy. Soc. (London) **A277**, 297 (1963).

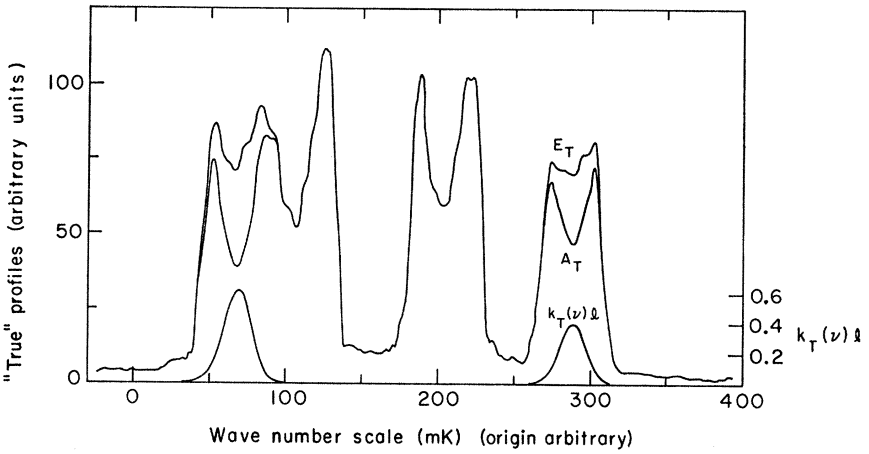

FIG. 19. "True" emission (E_T) and absorption (A_T) profiles for Rb^{87}, found by guessing a true emission profile, convolving it with an instrument function of finesse 25 and $R=0.935$, and comparing the convolution with the experimental data (Fig. 5) to obtain corrections to improve the trial profile. After good agreement is obtained between the convolved profile and the data, the true absorption profile is obtained by multiplying the true emission profile by $\exp[-k_T(\nu)l]$. The shape of $k_T(\nu)$ is known theoretically, and the scale factor is chosen to give good agreement between the predicted and experimental absorption profiles (see Fig. 20).

each frequency in the direction needed to make the convolved profile agree with the observed profile at the same frequency. With even a very rough first-guess function, less than ten iterations were usually needed to produce a trial function whose convolution agreed with the observed emission profile to within 1% of the peak value at every frequency. The "true" emission function corresponding to Fig. 5 is shown in Fig. 19. An instrument function of finesse 25 and reflection coefficient 0.935 was used in the unconvolving calculations.

We tried a more elegant approach to remove the effects of the instrument function on the absorption coefficient. It is well known that the Fourier transform of the convolution integral of two functions is merely the product of the Fourier transforms of the functions.[33] Hence the ratio of (a) the Fourier transform of the recorded output of the Fabry-Perot interferometer to (b) the transform of the (measured) instrument function gives the transform of the input spectrum. This method was modified[34] to account for the periodicity of the instrument function of the Fabry-Perot; this periodicity makes the function expressible more easily as a Fourier series. This procedure was highly satisfactory for computer-generated (essentially noise-free) data, but failed to give consistent results with real (noisy) data. As pointed out by other authors,[35] what is needed is either some method for smoothing the data before transforming or some method of apodization to reduce the contribution of the high-frequency Fourier components (which come mainly from the noise in the data).

3. *Predicted Absorption Profile*

We found $k_T(\nu)$ by summing Gaussians of the proper width [(Eq. (29)], separation, and relative intensities. Then by (6) we obtained the true absorption profile; see, for example, Fig. 19. The predicted emission and absorption profiles were found by convolving the true profiles with the instrument function (Figs. 20 and 21). The predicted emission profile was, of course, forced to agree well with the observed profile. However, the theory then fixed the predicted absorption profile except for the over-all scale factor which multiplies $k_T(\nu)$. That this single parameter could be chosen to give good agreement between the predicted and observed absorption profiles at all frequencies is taken as convincing evidence that this approach is indeed valid. A similar analysis was carried out for one of the highest densities occurring in the experiment.

4. *Corrections Yielding $k_T(\nu_0)$ from $k_P(\nu_0)$*

The model case described in the preceding paragraph gives the relation between a single density or $k_T(\nu_0)$ and the predicted peak coefficients. Corrections for other densities are found by: (1) changing $k_T(\nu)$ by an over-all scale factor, (2) computing the new true absorption profile from $k_T(\nu)$ and the true emission profile (unchanged), and (3) computing the predicted emission and absorption profiles and the predicted peak absorption coefficient, $k_P(\nu_0)$. Curves of the true versus the predicted absorption coefficients can then be plotted as in Fig. 22, which demonstrates the dependence of the corrections upon finesse (or the instrumental width when a fixed spacer is used) and reflection coefficient.

5. *Summary of Density-Measurement Analysis*

From a Fabry-Perot scan, the observed composite peak-absorption coefficient (for example, the *efg* component of Rb^{87}) was determined. From it the true composite peak coefficient was found by means of a correction curve such as Fig. 22, by setting the observed coefficient equal to the predicted coefficient. If, as in Fig. 20, equating the peak predicted and observed coefficients did not give the best over-all fit to the absorption profile, an additional correction of a few percent was

[33] P. M. Morse and H. Feshbach, *Methods of Theoretical Physics* (McGraw-Hill Book Company, New York, 1953), p. 464.

[34] The extensive contribution of Professor E. L. O'Neill in setting up this problem in a form suitable for solution on a digital computer is gratefully acknowledged.

[35] J. D. Morrison, J. Chem. Phys. **39**, 200 (1963). Charles A. Whitney, Astrophys. J. **137**, 327 (1963).

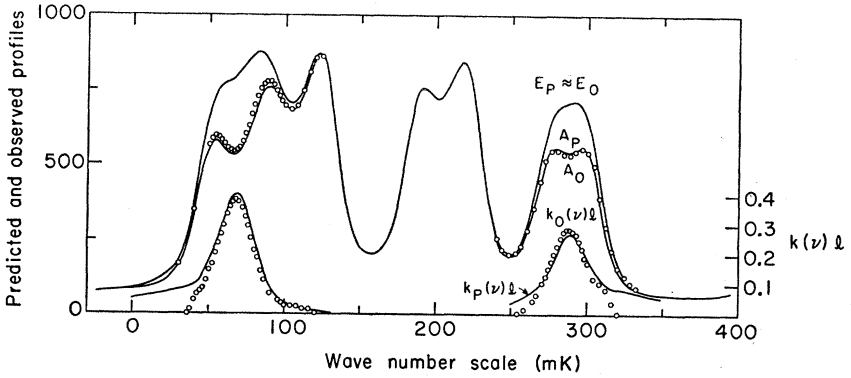

FIG. 20. Predicted and observed profiles for Rb^{87} absorption of light from a natural-Rb lamp corresponding to Figs. 5 and 19. Since the predicted values of the emission profile E_P are forced to agree (to within 1% of the peak) with the observed profile E_0, only the former is plotted. Because an unnormalized instrument function was used in the convolution, no comparison of absolute intensity should be made between this figure and Fig. 19. The upper open circles are the experimentally observed values of the absorption profile A_0; the lower open circles are the observed values ot the absorption coefficient times the cell length. Parameters defining the instrument function: convolution of Airy function (=0.935) and Gauss function (width 11.1 m K, F_σ=420 mK).

necessary to yield the best estimate of the true peak coefficient. From the true composite peak coefficient and the frequency dependence of $k_T(\nu)$, the density could be found with (5). In the Rb runs, only the *efg* composite peaks were used; in Cs the average of all four single peaks was used. Implicit in the use of these corrections was that the lamp profile be little changed from its condition in the model case. This requirement was satisfied by the lamp used in this experiment.

6. *Comparison with Results of* $\int k_0(\nu)d\nu$ *Method*

Figures 20 and 21 contain plots of the predicted and observed absorption coefficients. The predicted values lie above the observed values away from the peaks, because the differences between small numbers were lost in the experimental noise. The integral of the predicted coefficient is often much larger than the integral of the true coefficient.[26] Under the conditions of this experiment, the integrals of the observed and true coefficients agreed fairly well for low densities, but disagreed appreciably at higher densities; see Table I. It is ironical that, as the experimental technique is improved so that the differences between the small numbers between peaks become measurable, the estimate of the density found by taking the integral of the observed coefficient actually becomes worse.

7. *Cross Check by the Equivalent-Width Method*

In order to test the reliability of the density measurement, we made an independent determination by the equivalent-width method.[36] "White" light from a Sawyer 500 projector passed through the cell and was detected by a scanning monochromator (Jarrell-Ash $\frac{1}{2}$-meter). Whenever the scan traversed an absorption line, the transmitted intensity was decreased as in Fig. 23. The very nearly triangular shape of the absorption corresponded to the rectangular instrument function of the monochromator determined by the 25-μ slits.

If the intensity of the incident radiation is constant over several instrument widths, $f(\nu')$ in Eq. (7) is independent of frequency and

$$I_0(\nu)=f\int g(\nu-\nu')d\nu'=I_0. \tag{30}$$

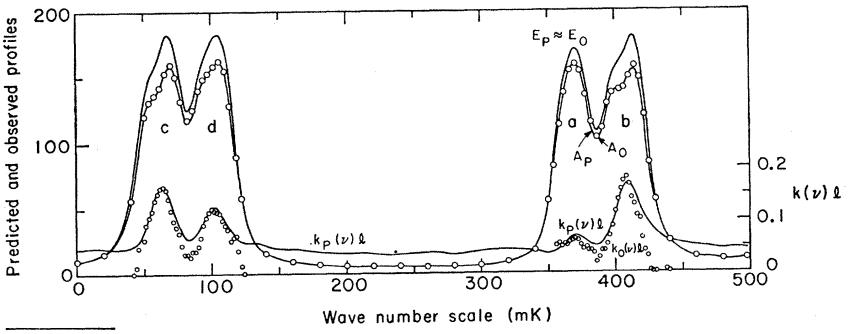

FIG. 21. Predicted and observed profiles for Cs^{133}. Instrument function: convolution of Airy (R=0.95) and Gauss (width 11.7 mK, F_σ=500 mK).

[36] E. W. Foster, Rept. Progr. Phys. **27**, 469 (1964).

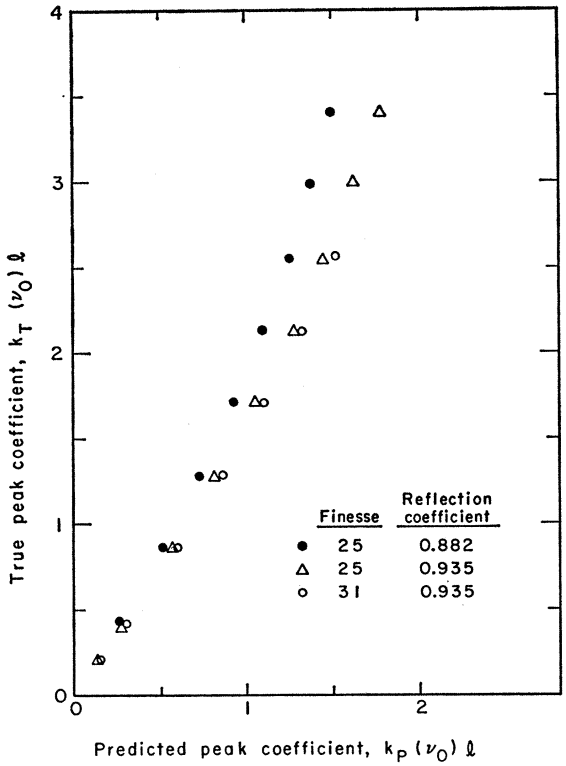

FIG. 22. True and predicted absorption coefficients for the composite *efg* peak of Rb^{87}. The predicted coefficients are obtained from predicted emission and absorption profiles resulting from the convolution of an instrument function (defined by the finesse and reflection coefficient given above) with the true profiles of Fig. 19. Correction curves such as these are used to find the true peak coefficient—and hence the density—from the observed composite peak.

A quantity A can then be defined as

$$A=\int_{\nu_1}^{\nu_2}[I_0(\nu)-I_0'(\nu)]d\nu/I_0, \tag{31}$$

where the absorption of the line of interest is negligible outside the interval ν_1 to ν_2. Under these conditions A is independent of the limits of integration, and is also independent of the instrumental profile and width.

$$A=\nu_2-\nu_1-\int\int_{\nu_1}^{\nu_2} fg(\nu-\nu')\exp[-k_T(\nu')l]d\nu'd\nu/I_0 \tag{32}$$

$$=\nu_2-\nu_1-\int_{\nu_1}^{\nu_2}\exp[-k_T(\nu')l]d\nu'. \tag{33}$$

If the shape of $k_T(\nu')$ is known, a correction curve of A versus $k_T(\nu_0)$ or the density can be found; see Fig. (24). For high absorption, the natural broadening contributions to $k_T(\nu)$ become important in determining A, but this effect was negligible in this experiment.

The Fabry-Perot method becomes less reliable at high densities because of the increase in the fractional corrections. On the other hand, with the equipment described above, the equivalent-width measurement was inaccurate at low densities because the signal was small. However, the equivalent-width method is independent of detailed information about the instrument function. Also since a white-light source must be used, one has no problem in regaining the true emission profile as in the Fabry-Perot case. Both methods require a knowledge of the lifetime of the relevant states and the details of the absorption lines.

Table II compares the density measurements made by both methods. We believe the equivalent-width values to be accurate to 15 or 20%, because of lamp

TABLE I. Comparisons of densities estimated by the $k(\nu_0)$ and $\int k_0(\nu)d\nu$ methods. Densities are in units of 10^{10} atoms per cm^3.

Sidearm temperature	24°C	41°C
Isotope	Rb^{87}	Rb^{87}
Component	7800 Å: *e*, *f*, *g*	7800 Å: *e*, *f*, *g*
n by $k(\nu_0)$ method	0.79	5.5
n by $\int k_0(\nu)d\nu$ method	0.86	6.9

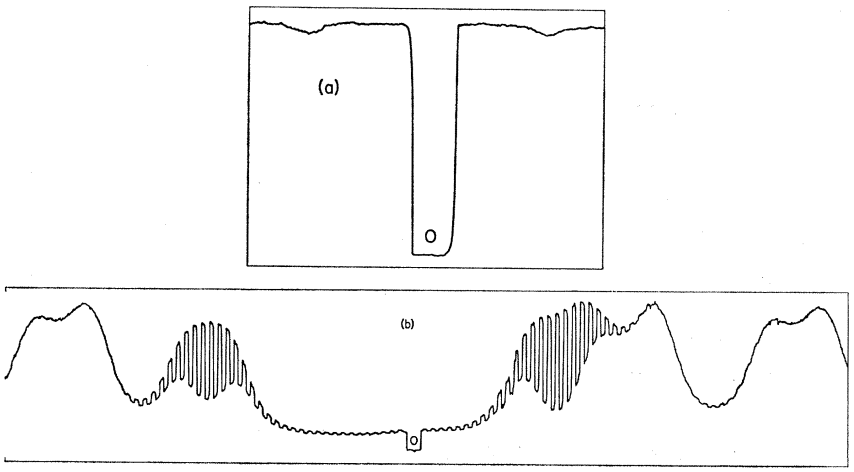

FIG. 23. Typical data from the comparison of the equivalent-width and Fabry-Perot density measurements taken at the same density. (a) Equivalent-width scan of 7947 Å line. (b) Fabry-Perot scan of 7800 Å line.

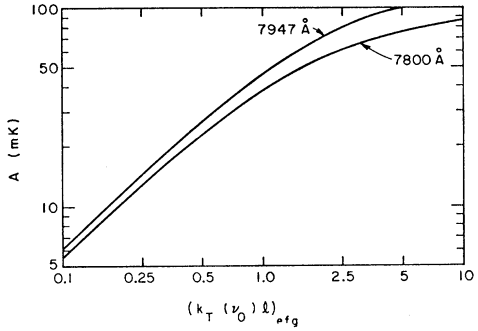

FIG. 24. Curves of growth showing A, defined by Eqs. (31) to (33), as a function of the Rb^{87} efg composite peak of the true absorption coefficient, which is proportional to the density.

fluctuations, noise, and lack of reproducibility. The lack of serious disagreement between the two methods, which differ considerably in technique and analysis, is reassuring.

VI. SUMMARY OF RESULTS

For the self-exchange experiments, the values of $1/\tau$ were least-squares-fitted to

$$1/\tau=[1/\tau']+B_{S1}p, \tag{34}$$

where τ' is the non-spin-exchange relaxation time, B_{S1} is defined by (3), and p is the density. For cross exchange, a term $B_{E1}d$ was added to (34). The data points and best-fit curves are given in Fig. 25 for run 7 in Rb^{87}, and in Fig. 26 for run 8 in Rb^{87}-Cs^{133}. The results of the Rb^{87} and Cs runs are summarized in Tables III and IV. Runs 5 through 8 were performed with a cubical cell about 5 cm on each internal edge; runs 9 and 11 used a 2.5 by 5 by 5 cm cell, with the density measured along the short path length. In the Rb^{87}-Cs^{133} run, p was held fixed and the term $B_{S1}p$ was included in $1/\tau'$. Run 11 between Rb^{87} and Rb^{85} supports the results of others[12,37] that the Rb^{87}-Rb^{85} cross section is approximately equal to the Rb^{87}-Rb^{87} cross section; the difference, if any, is within the uncertainty of these measurements.

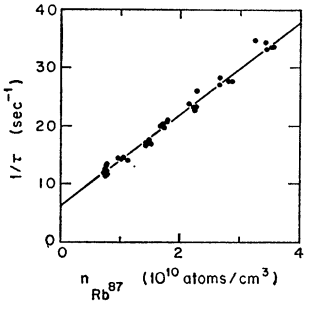

FIG. 25. Summary of run 7 Rb^{87}-Rb^{87} spin-exchange cross-section measurement by hyperfine pumping. $1/\tau=A+Bn$, $A=6.2\pm0.2$ sec^{-1}, $B=(7.9\pm0.2)\times10^{-10}$ cm^3/sec.

[37] T. Carver, Proceedings of the Ann Arbor Conference on Optical Pumping, 1959, p. 29 (unpublished).

The errors on the parameters in the figures and tables are standard deviations of external consistency deduced from statistical considerations alone. The random errors were only a few percent. In order to account for the possibility of systematic errors, the standard deviations for the cross sections were increased to 10% of the value. This choice was, of course, arbitrary, but is believed to be a conservative estimate.

We estimate that the systematic errors associated with the $1/\tau$ measurements were less than 5%. The time base determined by the signal generators, measured by an electronic counter (Hewlett Packard 5245L), was found to be stable, after warmup, to better than 1%. The linearity of the system was checked repeatedly. The relaxation time was insensitive to the particular oscilloscope scale and to the setting of the take-data point (bright spots in Fig. 3) over a reasonable range of a few tenths of a millisecond. The more troublesome problems of the Kerr cell and detector have presumably been adequately solved. Scattered light effects were negligible in both the relaxation-time and density measurements. The principal source of possible systematic error in the relaxation-time analysis was in the estimation of the polarization used in correcting for the cell-length effect. But the polarization was probably known to 25% of its value or better. This corresponds to a maximum error of 3% in $1/\tau$.

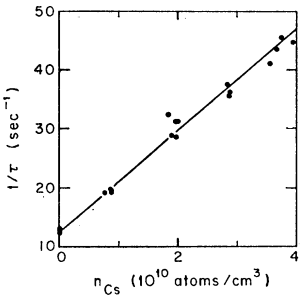

FIG. 26. Summary of run 8 Rb^{87}-Cs^{133} spin-exchange cross-section measurement obtained by hyperfine pumping. $1/\tau=A+Bn$, $A=13.1\pm0.1$ sec^{-1}, $B=(8.7\pm0.2)\times10^{-10}$ cm^3/sec.

The density-measurement systematic error is expected to be about 5 or at most 10%. The density-measurement analysis was internally consistent; it gave good predictions of relative absorption probabilities, absorption widths, and over-all profiles. It is also in reasonable agreement with the equivalent-width method.

In order that the cross section be proportional to the slope of the $1/\tau$ versus density curve, $1/T_1'+1/T_1''$ in Eq. (2) must be independent of the densities. The slow decrease in relaxation time with exposure to high densities would violate this restriction. Consequently, the data at high densities were taken rapidly and then data at low densities were taken and compared with previous low-density data. If the low-density sets agreed, little change in the relaxation time could have occurred at the high density since reducing the density was not sufficient to restore the original relaxation time.

TABLE II. Comparison of density measurements by the Fabry-Perot and equivalent-width methods. The numbers are Rb^{87} densities in units of 10^{10} cm^{-3}.

Sidearm temperature (°C)	Fabry-Perot method *efg* component of 7800 Å	Equivalent-width method 7947 Å	7800 Å	Average
33–34	2.8±0.3	2.96	3.76	3.4±0.7
46–47	5.6±0.6	6.00	5.28	5.6±1.1
54–55	7.4±0.7	8.68	7.40	8.0±1.6

If the low-density sets disagreed, the run was rejected.

One might also imagine a more subtle density dependence in which the relaxation rate varied directly as the alkali density. Such a mechanism was proposed by Berg to account for observations with the atomic-hydrogen maser.[38] We believe that such a dependence was not present because: (a) the observed relaxation rate appeared to be dominated by effusion from the cell into the sidearms, (b) the results for the two cells of different size were consistent, and (c) the results were consistent from day to day and from coating to coating. A crude estimate of the relaxation rate from effusion into the sidearms agrees well with the measured rate.[15] As calculated, the relaxation time was longer in the smaller cell because the openings to the sidearms were smaller. Furthermore, melting the coating always restored the same relaxation time; if the relaxation were dominated by wall imperfections, a different rate would be expected after each melting.

TABLE III. Summary of Rb^{87}-Rb^{87} total spin-exchange cross-section measurements.

Experiment and reference	$B_{S1}=\int\int\lvert f_t-f_s\rvert_{S1}^2 d\Omega \times v_{S1} f(v_{S1}) d^3v_{S1}/4$ (10^{-10} cm^3 sec^{-1}) at 78±5°C	$\sigma=B/\bar{v}_{S1}$ (10^{-14} cm^2)
Carver[a]		1.5–2.6
Moos and Sands[b]		2.6 ±0.4
Jarrett (Rb^{87}-Rb^{85})[c]		1.85±0.23[d]
Davidovits and Knable[e]		1.70±0.20[f]
Bouchiat and Brossel[g]		2.2
This experiment[h] (Gibbs and Hull): (with $\tau_{Rb(D_2)}=0.278$ nsec)		
Run 5	7.4±0.2	1.79±0.05
Run 6	8.2±0.5	1.99±0.12
Run 7	7.9±0.2	1.90±0.05
Run 9	8.1±0.2	1.95±0.06
Average (weighted)	7.9±0.2	1.91±0.04
Average with increased error as an estimate of possible systematic errors	7.9±0.8	1.9 ±0.2

[a] Reference 37. Also see note added in proof.
[b] Reference 9.
[c] Reference 10.
[d] In the value quoted by Jarrett, $\sigma=B/v_{rms}$ was assumed, whereas here $\sigma=B/\bar{v}$; therefore Jarrett's quoted value has been increased by $v_{rms}/\bar{v}$ for easy comparison.
[e] Reference 11.
[f] The authors have been informed by Davidovits that the cross section reported in Ref. 11 and quoted in Ref. 15 should be multiplied by 2, using the definition of the spin-exchange cross section given in Refs. 13 and 15.
[g] Reference 12. Also see note added in proof.
[h] The errors for each run are standard deviations of external consistency obtained from statistical considerations alone. The standard deviation for the average is

$$\left[\sum_{i=1}^{n}(\sigma_i-\bar{\sigma})^2/n(n-1)\right]^{1/2},$$

where n is the number of cross sections σ_i to be averaged.

[38] H. C. Berg, Phys. Rev. 137, A1621 (1965).

TABLE IV. Summary of Rb^{87}-Cs^{133} total spin-exchange cross-section measurements.

Experiment and reference	$B_{E1}=\int\int\lvert f_t-f_s\rvert_{E1}^2 d\Omega \times v_{E1} f(v_{E1}) d^3v_{E1}/4$ (10^{-10} cm^3 sec^{-1}) at 78±5°C	$\sigma=B/\bar{v}_{E1}$ (10^{-14} cm^2)
Bouchiat and Grossetête[a]		2.4 ±0.4
This experiment[b] (Gibbs and Hull): (with $\tau_{Cs(D_1)}=0.312$ nsec)		
Run 8	8.6±0.2	2.28±0.05
Value including possible systematic errors	8.6±0.9	2.3 ±0.2

[a] F. Grossetête, Compt. Rend. 259, 3211 (1964); 258, 3668 (1964); M. A. Bouchiat and F. Grossetête, J. Phys. Radium 27, 353 (1966).
[b] The value of the cross section differs from that given in Ref. 15 because of our improved density-measurement analysis of Part VB and the use of a better value for the Cs lifetime.

The analysis of the data then indicate that at 78°C

$$\sigma(Rb^{87}\text{-}Rb^{87})=(1.9\pm0.2)\times10^{-14}\text{ cm}^2,$$

$$\sigma(Rb^{87}\text{-}Cs^{133})=(2.3\pm0.2)\times10^{-14}\text{ cm}^2.$$

From the theoretical results of Dalgarno and Rudge,[39] who state that their values may be underestimations of as much as 30%, one can easily calculate theoretical values of the above cross sections to be 1.68×10^{-14} and 1.84×10^{-14} cm^2, respectively.

Note added in proof. We have been quoting 4–7 (units of 10^{-14} cm^2) for Carver's Rb^{87}-Rb^{87} cross section and 6 for that of Bouchiat and Brossel. However, Brossel has kindly drawn our attention to the second of Ref. 12, in which it is pointed out that more than one vapor-pressure curve exists in the literature for Rb. The cross sections first published by both groups utilized a vapor-pressure curve now believed to be incorrect. The cross sections in Table III were deduced from the presently accepted curve. We find it quite gratifying that the results of Table III are in such good agreement, considering the wide variety of techniques represented. The recently remeasured [John K. Link, J. Opt. Soc. Am. 56, 1195 (1966)] values of the Rb $5p^2P_{3/2}$ and Cs $6p^2P_{1/2}$ lifetimes are 28.1±0.5 and 34.0±0.6 nsec, respectively. This leads to σ (Rb^{87}-Cs^{133}) = (2.1±0.2) $\times10^{-14}$ cm^2. The ratio of the Rb-Cs and Rb-Rb cross sections is then in better agreement with the prediction of Dalgarno and Rudge.[39]

ACKNOWLEDGMENTS

The authors express their appreciation to the following: Professor Alfred Glassgold for suggesting a study

[39] A. Dalgarno and M. R. H. Rudge, Proc. Roy. Soc. (London) A286, 519 (1965).

of the spin-exchange process, Dr. Joseph Winocur for suggesting the use of the Franzen technique in cross-section measurements and for assisting with the early work, Professor Howard Shugart for assistance with electronics and computer problems, Dr. John Link for pointing out the equivalent-width method of density measurement, Dr. Lee Bradley, III, and Prof. E. L. O'Neill for helpful discussions of the density-measurement analysis, Morely Corbett and Robert Sedlack for the construction of many pieces of glass apparatus, and Dan O'Connell for his superb service in coating the Fabry-Perot plates.

APPENDIX: THEORY OF THE HYPERFINE EXPERIMENT

The expression for the signal for the hyperfine experiment is derived as an extension of the previous calculations for Zeeman experiments.[13] The significant differences between the present assumptions and those of Part II of the Zeeman paper are: (a) the hyperfine components in the incident light are assumed to be unequal here, although transitions from different hyperfine levels of the same excited fine-structure state to a given ground-state hyperfine level are assumed to be unresolved in absorption; (b) circularly polarized D_2 light is included as well as D_1 light in the pumping radiation; (c) an rf field is continuously applied to the first species as well as to the second in order to nullify any Zeeman pumping; (d) the low-absorption requirement is made less stringent. As before, we assume that no buffer gas is present, so that the populations are essentially independent of position in the cell.

As in Eq. (7) of Ref. 13, the change between x and $x+dx$ in the intensity of light (arising from the transition from one of the hyperfine levels of the excited J_1' state to the ground-state hyperfine level F_1) of frequency ν is given by

$$dL_{F_1}{}^{J_1'}(\nu,x,t)=-L_{F_1}{}^{J_1'}(\nu,x,t)\sum_{M_1F_1'}p_{F_1M_1}(x,t)\times P_\nu'(F_1M_1,J_1'F_1'M_1+1)h\nu dx, \quad \text{(A1)}$$

assuming that the incident light is circularly polarized in such a way that M_1' must equal M_1+1 for absorption to occur. The density in the F_1M_1 ground-state sublevel is $p_{F_1M_1}$. Here P_ν' is proportional to the absorption probability for the transition F_1M_1 to J_1', F_1', M_1+1 at frequency ν. In a cell with no buffer gas and low density of atoms, the atoms traverse the cell in a time that is short compared with the other times in the experiment. Hence $p_{F_1M_1}(x,t)=p_{F_1M_1}(t)$ is independent of x. Furthermore, if an rf field is applied at the proper frequency, the magnetic sublevels in each hyperfine level are equally populated:

$$p_{F_1M_1}(x,t)=p_{F_1}(t)/(2F_1+1). \quad \text{(A2)}$$

Also

$$d_{F_2M_2}(x,t)=d_{F_2}(t)/(2F_2+1), \quad \text{(A3)}$$

where $d_{F_2M_2}$ is the density in the F_2M_2 sublevel of a second species that may be present.

Integrating (A1) over x yields

$$L_{F_1}{}^{J_1'}(\nu,x,t)=L_{F_1}{}^{J_1'}(\nu,0)\exp\left\{-\sum_{M_1F_1'}\left[\frac{p_{F_1}(t)}{2F_1+1}\right]\times P_\nu'(F_1M_1,J_1'F_1'M_1+1)h\nu x\right\}. \quad \text{(A4)}$$

But for thermal equilibrium

$$p_{F_1}\approx(2F_1+1)p/2(2I_1+1)\equiv p_{F_1}(\infty) \quad \text{(A5)}$$

and

$$L_{F_1}{}^{J_1'}(\nu,x,t)=L_{F_1}{}^{J_1'}(\nu,0)\exp[-k_T(\nu)|_{F_1}{}^{J_1'}x]. \quad \text{(A6)}$$

The absorption coefficient is independent of the direction and polarization of the light, provided the magnetic sublevels of each hyperfine level are equally populated.[40] Then (A4) can be rewritten as

$$L_{F_1}{}^{J_1'}(\nu,x,t)=L_{F_1}{}^{J_1'}(\nu,0)\times\exp\{-p_{F_1}(t)k_T(\nu)|_{F_1}{}^{J_1'}x/p_{F_1}(\infty)\}. \quad \text{(A7)}$$

The absorption is then

$$A_{F_1}{}^{J_1'}(\nu,t)=L_{F_1}{}^{J_1'}(\nu,0)-L_{F_1}{}^{J_1'}(\nu,l,t) \quad \text{(A8)}$$

$$=L_{F_1}{}^{J_1'}(\nu,0)[1-\exp\{-k_T(\nu)|_{F_1}{}^{J_1'}l\}\times\exp\{-P_{F_1}(t)k_T(\nu)|_{F_1}{}^{J_1'}l\}], \quad \text{(A9)}$$

where

$$P_{F_1}(t)\equiv[p_{F_1}(t)-p_{F_1}(\infty)]/p_{F_1}(\infty), \quad \text{(A10)}$$

Equation (A10), the fractional deviation of the density of the F_1 hyperfine level from its thermal equilibrium value, is called the polarization of the F_1 level. In the limit that all atoms are pumped out of the $F_1=I_1+\frac{1}{2}$ state, $P_+(0)$ is -1. The signal may be defined as

$$S(t)=\sum_{F_1J_1'}\int[A_{F_1}{}^{J_1'}(\nu,\infty)-A_{F_1}{}^{J_1'}(\nu,t)]d\nu\Big/\sum_{F_1J_1'}\int[A_{F_1}{}^{J_1'}(\nu,\infty)-A_{F_1}{}^{J_1'}(\nu,0)]d\nu. \quad \text{(A11)}$$

The numerator of (A11) is the difference between the absorption at time t and at a time much longer than the relaxation time. The integral over frequency extends over the frequencies of the J_1' to F_1 transition. The summation accounts for the fact that both ground-state hyperfine components of both D lines can reach the detector. Then

[40] E. V. Condon and G. H. Shortley, *The Theory of Atomic Spectra* (Cambridge University Press, London, 1959), p. 102.

in general

$$S(t)=\frac{\sum_{F_1J_1'}\int L_{F_1}{}^{J_1'}(\nu,0)\exp[-k_T(\nu)|_{F_1}{}^{J_1'}l]\{1-\exp[-P_{F_1}(t)k_T(\nu)|_{F_1}{}^{J_1'}l]\}d\nu}{\sum_{F_1J_1'}\int L_{F_1}{}^{J_1'}(\nu,0)\exp[-k_T(\nu)|_{F_1}{}^{J_1'}l]\{1-\exp[-P_{F_1}(0)k_T(\nu)|_{F_1}{}^{J_1'}l]\}d\nu}. \tag{A12}$$

If the product of the polarization P_{F_1} and the optical thickness of kl is small compared to 1, the exponential can be expanded and (A12) replaced by the approximate signal

$$S_A(t)=\sum_{F_1J_1'}\int L_{F_1}{}^{J_1'}(\nu,0)\exp[-k_T(\nu)|_{F_1}{}^{J_1'}l]P_{F_1}(t)k_T(\nu)|_{F_1}{}^{J_1'}ld\nu\Big/$$
$$\times\sum_{F_1J_1'}\int L_{F_1}{}^{J_1'}(\nu,0)\exp[-k_T(\nu)|_{F_1}{}^{J_1'}l]P_{F_1}(0)k_T(\nu)|_{F_1}{}^{J_1'}ld\nu$$
$$=P_+(t)/P_+(0), \tag{A13}$$

since $P_-(t)=-p_+(\infty)P_+(t)/p_-(\infty)$, where $+$ and $-$ refer to $F_1=I_1\pm\frac{1}{2}$. Notice that for $l=0$, (A12) and (A13) are equal; the correction to account for their difference can then be logically termed the cell-length correction.

At any rate the signal is a function of $p_+(t)$. If (A13) is applicable, then only $p_+(t)$ is needed; but if (A12) must be used, further information about the light profile and the initial polarization is required.

The time dependence of p_+ can be found as follows: For the hyperfine-pumping experiment using the Franzen method of detection, Eq. (1) of Ref. 13 becomes [by summing over M_1 and using (28), (31), (32), (43), (45), (59), (61), (A2), and (A3) of that paper]:

$$\dot{p}_{F_1}=-\sum_{F_1'M_1'M_1}\Delta(F_1,F_1')\left[\frac{(2I_1+1)^2\delta_{F_1,F_1'}}{T_1}+\frac{1}{T_1'}\right]\begin{pmatrix}F_1' & 1 & F_1\\ -M_1' & M_1'-M_1 & M_1\end{pmatrix}^2\frac{[p_{F_1}/(2F_1+1)-p_{F_1'}/(2F_1'+1)]}{4}$$
$$-\frac{p_{F_1}}{T_1''}+\frac{(2F_1+1)p}{2(2I_1+1)T_1''}-\sum_{\substack{M_1F_2M_2\\F_1'M_1'F_2'M_2'}}\Delta(F_1,F_1')\Delta(F_2,F_2')\sum_q\begin{pmatrix}F_1' & 1 & F_1\\ -M_1' & q & M_1\end{pmatrix}^2\begin{pmatrix}F_2' & 1 & F_2\\ -M_2' & -q & M_2\end{pmatrix}^2$$
$$\times\frac{[p_{F_1}d_{F_2}/(2F_1+1)(2F_2+1)-p_{F_1'}d_{F_2'}/(2F_1'+1)(2F_2'+1)]}{4T_{E1}d}-\sum_{\substack{M_1F_1'M_1'\\F_1''M_1''F_1'''M_1'''}}\Delta(F_1,F_1'')\Delta(F_1',F_1''')$$
$$\times\sum_q\begin{pmatrix}F_1''' & 1 & F_1\\ -M_1'' & q & M_1\end{pmatrix}^2\begin{pmatrix}F_1'' & 1 & F_1'\\ -M_1'' & -q & -M_1'\end{pmatrix}^2$$
$$\times\frac{[p_{F_1}p_{F_1'}/(2F_1+1)(2F_1'+1)-p_{F_1''}p_{F_1'''}/(2F_1''+1)(2F_1'''+1)]}{4T_{S1}p}. \tag{A14}$$

By Edmonds[41] Eqs. (3.7.8) and (6.2.9),

$$\dot{p}_{F_1}=-p_{F_1}/T_1''+(2F_1+1)p/2(2I_1+1)T_1''$$
$$+(1/T_1'+1/T_{E1}+1/T_{S1})[-3p_{F_1}+\sum_{F_1'}p_{F_1'}\Delta(F_1,F_1')/(2F_1'+1)]/4. \tag{A15}$$

With $p_-=p-p_+$ and with Table II of Ref. 13, we see that

$$\dot{p}_+=-(1/T_1'+1/T_1''+1/T_{E1}+1/T_{S1})p_++(2I_1+2)(1/T_1'+1/T_1''+1/T_{E1}+1/T_{S1})p/2(2I_1+1). \tag{A16}$$

Equation (2) follows easily from (A16) and (A13).

[41] A. R. Edmonds, *Angular Momentum in Quantum Mechanics* (Princeton University Press, Princeton, New Jersey, 1957).

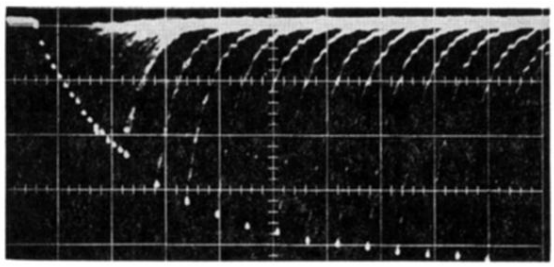

FIG. 13. Typical hyperfine pumping and relaxation transients in Rb^{87}. Absorption cell at 24°C, run 5.

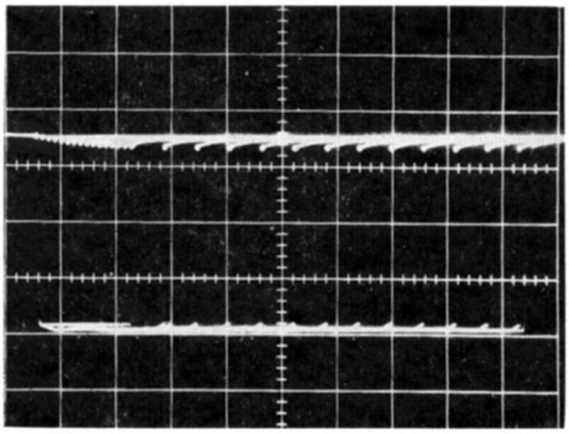

FIG. 2. Total light signal obtained with hyperfine pumping (5 mV/cm, 25 msec between long off intervals, 5 msec between short off intervals).

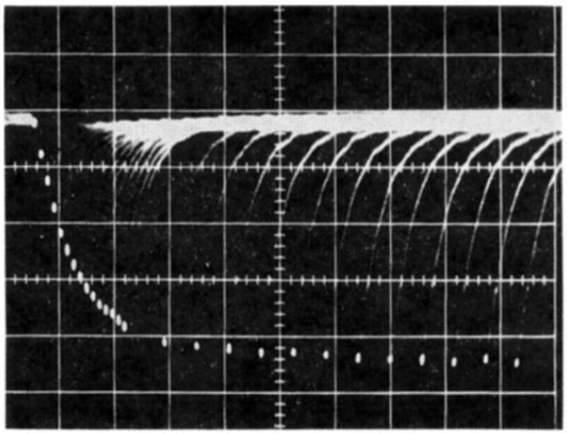

FIG. 3. The top of Fig. 2 with the vertical axis amplified 25 times (0.2 mV/cm).